DESIGN OF A MODIFIED AFM SETUP WITH MINIATURIZED-MAGNETIC PARTICLE ACTUATORS FOR BIOMOLECULAR APPLICATIONS

The Institute for Graduate Studies

in

Science and Engineering

Boğaziçi University

DESIGN OF A MODIFIED AFM SETUP WITH MINIATURIZED-MAGNETIC PARTICLE ACTUATORS FOR BIOMOLECULAR APPLICATIONS

by

Semih Sevim

B.S., Mechanical Engineering, Boğaziçi University, 2013

Submitted to the Institute for Graduate Studies in
Science and Engineering in partial fulfillment of
the requirements for the degree of
Master of Science

Graduate Program in Mechanical Engineering

Boğaziçi University

2016

ACKNOWLEDGEMENTS

First and foremost, I would like to express my appreciation to my thesis advisor and co-advisor, Assoc. Prof. Hakan Ertürk and Assist. Prof. Hamdi Torun, respectively, for their guidance and support throughout my research and thesis. I have always felt the pleasure of being a member of Bio-AFM Laboratory under the supervision of Assist. Prof. Hamdi Torun. With his knowledge and experience in the field of microsystems and atomic force microscopy (AFM) it has become possible for me to reach Master of Science. I would like to thank Assoc. Prof. Çetin Yılmaz, Assoc. Prof. Arda Deniz Yalçınkaya and Assist. Prof. Baykal Sarıoğlu for sharing their knowledge and taking part in my thesis jury. I would like to also sincerely thank Assoc. Prof. Yalçınkaya for giving me a chance to use his laboratory and equipment (MNL) during characterization processes and preparation of experimental apparatus. I am deeply appreciated with my research partner, Dr. Sevil Özer for her help, support, motivation and friendship in this work. Without her it would be much more difficult to achieve. Together with her I would like to thank Feng Luying for her help in software design phases. I would like to give my acknowledgement to Microsystem Based Medical Device Development Center of Boğazici University Life Sciences and Research Center where the prototypes were manufactured. I would like to thank my colleagues from MSRL Laboratory in Swiss Federal Institute of Technology in Zurich (ETHZ) for supplying the electromagnet and magnetic particles, and colleagues from University of Würzburg for supplying biomolecules.

I would also like to thank The Scientific and Technological Research Council of Turkey (TÜBİTAK) for providing scholarship through my study.

Last but not least, I owe my deepest gratitude to every special and precious person in my life, especially to my dearest parents and my dear friend Dilek Pehlivan for their emotional support during my graduate study in Boğaziçi University.

This research is supported with funding from the EC (ICT FET-Open) under the MANAQA Project, Grant no 296679.

ABSTRACT

DESIGN OF A MODIFIED AFM SETUP WITH MINIATURIZED-MAGNETIC PARTICLE ACTUATORS FOR BIOMOLECULAR APPLICATIONS

In this thesis, design and characterization of a new atomic force microscopy (AFM) setup having conventional piezoactuator together with an electromagnetic actuator and a novel AFM technique using miniaturized-magnetic particles as an actuator for biomolecular experiments are presented. Jetted-polymers have been used in the mechanical assembly of AFM head, which allows rapid manufacturing. A PXI (Peripheral Component Interconnect, PCI extensions for Instrumentation) embedded controller programmed in NI-LabVIEW environment is used to drive the system. An integrated force resolution of 2 and 3 pN, respectively in air and in liquid is achieved in 1 kHz bandwidth with commercial cantilevers. In addition, a FeCo-tipped electromagnet provides high-force cantilever actuation with vertical magnetic fields up to 0.55 T. Temperature stabilization within 0.1° C is achieved using a Peltier cooler (TEC) to avoid the temperature increase due to the Joule heating of coil. Single-molecule experiments have been conducted using two different pairs of biomolecules (i.e. biotin/streptavidin and heparin/FGF-2). Both biomolecular pairs have been probed using conventional techniques (i.e. piezoactuation or electromagnetic actuation) on both commercial and new custom AFM system. In addition, a novel AFM technique is presented by manipulating functionalized magnetic microbeads using an electromagnet against a stationary AFM cantilever for advanced single-molecule force spectroscopy experiments. This method leads to a significant reduction of mechanical drift in the system since the experiments are performed without a need for a hard surface and the measured force between the cantilever and the bead is inherently differential. In addition, shrinking the size of the actuator can minimize hydrodynamic forces affecting the AFM cantilever. The new method reported herein allows applying constant force on the beads to perform force-clamp experiments without any active feedback.

ÖZET

BİYOMOLEKÜLER UYGULAMALAR İÇİN KÜÇÜLTÜLMÜŞ MANYETİK PARCACIK EYLEYİCİLİ MUADDEL ATOMİK KUVVET MİKROSKOBU TASARIMI

Bu tezde, geleneksel piezo eyleyicisi ile birlikte elektrikli mıknatıssal eyleyiciye sahip olan yeni bir atomik kuvvet mikroskobunun (AFM) tasarımı ve nitelendirmesi ve biomoleküler deneyler için küçültülmüş manyetik parcacıkların eyleyici olarak kullanıldıgı özgün bir AFM tekniği sunulmaktadır. AFM kafasını mekanik montajında fışkırtılmış polimer kullanılmıştır, bu da seri üretime izin vermektedir. NI-LabView ortamında programlanan bir PXI gömülü denetim birimi sistemi sürmek için kullanılır. Ticari manivelalar ile 1 kHz bant genişliği içinde 2 pN ve 3 pN bütünleşik kuvvet çözünürlüğüne, sırasıyla hava ve sıvı içerisinde ulaşılmıştır. Ek olarak, bir FeCo uçlu elektromıknatıs 0.55 Tesla'ya kadar dikey manyetik alan ile yüksek kuvvetli manivela tahriğini sağlamaktadır. Bobinin Joule ısınmasından dolayı olan sıcaklık artışını önlemek için, TEC kullanılarak sıcaklık istikrarı 0.1°C içinte başarılır. İki farklı çift biyomolekül kullanılarak, tek molekül deneyleri yürütülmüştür. Her iki biyomolekül çifti geleneksel yöntemler kullanılarak ticari ve yeni özel AFM sistemlerinde derinlemesine incelenmiştir. Ek olarak, İleri tek molekül kuvvet tayf ölçümü deneyleri için, özgün bir AFM yöntemi durağan bir manivelaya karşı elektromıknatıs kullanılarak yönlendirilen fonksiyonel haldeki manyetic micro-boncuklarla sunulmuştur. Bu yöntem sistemdeki mekanik sapmada önemli bir azalmaya yol açar, çünkü deneyler herhangi bir sert yüzeye gerek olmadan sergilenebilir ve manivela ile boncuk arasında ölçülen kuvvet tabiati gereği ayrışıktır. Ek olarak, eyleyicinin boyutunu küçültmek AFM manivelaları etkileyen hidrodinamik kuvvetleri küçültebilir. Burada bildirilen yeni yöntem herhangi bir aktif geri besleme olmadan kuvvet kelepçe deneyler gerçekleştirmek için boncuklar üzerinde sabit kuvvet uygulayanmasına izin verir.

TABLE OF CONTENTS

ACKNOWLEDGEMENTS iii
ABSTRACT iv
ÖZET v
TABLE OF CONTENTS vi
LIST OF FIGURES viii
LIST OF TABLES xiii
LIST OF SYMBOLS xiv
LIST OF ACRONYMS/ABBREVIATIONS xv
1. INTRODUCTION 1
2. DESIGN AND PROTOTYPE OF THE AFM SYSTEM 8
2.1. Hardware Design and Prototype of the AFM Head 9
2.2. Electromagnetic Actuator System Design and Prototype 12
2.3. Software-Electronic Design and User Interface 13
3. CHARACTERIZATION AND SYSTEM INTEGRATION 17
3.1. Characterization of the AFM Head 17
3.1.1. Noise Measurement of the AFM Head 17
3.1.2. Eigenfrequency Analysis with FEM 20
3.2. Characterization of the Electromagnetic Actuator System 23
3.2.1. Magnetic Characterization of AFM Head and the Electromagnatic Actuator System 24
3.3. System Integration 29
3.3.1. Temperature Control in Liquid Operation 31
3.3.2. Improvement in Drift Problem in AFM Measurements 32
4. BIOMOLECULAR EXPERIMENTS 34
4.1. Biomolecular Pulling Experiments Using Piezoactuator 36
4.1.1. Biotin/Streptavidin Force Spectroscopy Using Piezoactuator 37
4.1.2. Heparin/FGF-2 Force Spectroscopy Using Piezoactuator 42
4.2. Biomolecular Pulling Experiments Using Magnetically Actuated Cantilevers 44

4.3. Biomolecular Pulling Experiment Using Functionalized Magnetic Micropillars 46
4.4. Biomolecular Pulling Experiment Using Functionalized Magnetic Micro-Beads 49
4.4.1. Biotin/Streptavidin Force Spectroscopy Using Streptavidin Labeled Magnetic Beads 50
4.4.2. Heparin/FGF-2 Force Spectroscopy Using Heparin Labeled Magnetic Beads 51
4.4.3. Heparin Labeled Magnetic Beads Control Experiments 54
4.4.4. Effect of pH on Heparin/FGF-2 Unbinding Forces 55
4.4.5. Biomolecular Force Clamp Experiment without any Feedback Mechanism 56
5. CONCLUSION 59
REFERENCES 63

LIST OF FIGURES

Figure 1.1. a) Cantilever actuated and b) sample stage actuated AFM system. 1

Figure 1.2. A sample force curve and cantilever deflection schematics from a single-molecule interactions. 2

Figure 1.3. Schematic design of novel AFM system with bead actuation methodology..... 6

Figure 2.1. Schematic of the AFM system with dual actuation capability..... 8

Figure 2.2. a) Front and b) side views of the AFM head..... 10

Figure 2.3. Custom adapters for commercially available a) in-liquid, b) in-air cantilever holders. 10

Figure 2.4. The assembled AFM head. Laser path is drawn for illustrative purposes. .. 11

Figure 2.5. Designed AFM coil and sample holder for AFM body that allows applying translational force on magnetic micro-particles a) isometric view, b) Cross-sectional view. 12

Figure 2.6. Assembled AFM body with sample holder surface and electromagnet..... 13

Figure 2.7. Block diagram of the electronics for the AFM system. 14

Figure 2.8. User interface VI for AFM system..... 15

Figure 3.1. Force curve taken by actuating a silicon tip commercial cantilever (SNL10-D triangular, Bruker probes) using triangular piezo actuation over a silicon chip. 18

Figure 3.2. Power spectral density of a commercial cantilever (SNL10-D triangular, Bruker probes) in air (black curve) and in liquid (red curve). 19

Figure 3.3. Meshed AFM head assembly using Comsol Multiphysic 4.3b..... 20

Figure 3.4. Result of FEM simulations for specific Eigenmode in the AFM head. 21

Figure 3.5. FEM Eigen frequency analysis for a glass ceramic adaptor. 22

Figure 3.6. FEM Eigen Frequency Analysis for a structural steel adaptor. 23

Figure 3.7. a) The electromagnet is shown along with the micro-hall sensor which was used for characterizing the magnetic flux density. b) The experimentally measured vertical magnetic flux density is compared with FEM simulations at various current densities. 24

Figure 3.8. a) An electromagnet is placed under the AFM to see the magnetic actuation effects. b) Magnetic actuation of a commercial MFM cantilever (MESP, rectangular, Bruker Probes) in air with a square signal, having an amplitude of 300 mA at 1 kHz. 25

Figure 3.9. a) The picture of a soft magnetic micropillar, attached to a tipless AFM cantilever (CSC38-Tipless, Bruker Probes). Magnetic actuation of the micropillar attached cantilever b) with a zero mean sinusoidal input c) with a positive mean sinusoidal input. 26

Figure 3.10. Magnetic actuation of a commercial MFM cantilever (MESP, Bruker Probes) in air a) at 10 Hz and b) at 1 kHz using rectangular voltage drive signals. c) Force and current response graph with respect to frequency..... 28

Figure 3.11. a) Integrated AFM head with coil-sample holder, b) the manufactured AFM head with commercial elements, c) coil-sample holder. 29

Figure 3.12. Temperature trace of an immersed cantilever actuated using the electromagnet. The temperature starts rising when the electromagnet is turned on at t=5 min. The temperature controller is turned on at t=53 min to stabilize the temperature. 31

Figure 3.13. Time traces for the characterization of long time scale drift obtained using a commercial AFM (black) and magnetic actuation of a bead-attached cantilever (red). 33

Figure 4.1. Schematics of biomolecular pulling experiment with AFM. 35

Figure 4.2. Schematic of force spectroscopy experiment using piezoactuator and obtained sample curve. 37

Figure 4.3. A sample force curve a) showing a biotin/streptavidin interaction unbinding force about 80 pN with a loading rate of $3.3x10^4$ pN/s b) having no unbinding event. 38

Figure 4.4. Force histograms for the unbinding force levels of single biotin/streptavidin pairs obtained using custom AFM experiment. 39

Figure 4.5. a) A typical force curve exhibiting an unbinding event with a force strength ($F_{unbinding}$) of 75 pN. b) Another force curve indicating no adhesion/rupture events. 40

Figure 4.6. Force histograms for the unbinding force levels of single biotin/streptavidin pairs obtained using commercial AFM experiment. 40

Figure 4.7. Most probable rupture force versus loading rate graph, red scatter and black scatter correspond the custom AFM measurement and Commercial AFM measurements, respectively. 41

Figure 4.8. A sample force curve, a) showing a specific heparin/FGF-2 unbinding event, b) having no adhesion/rupture event. 43

Figure 4.9. The resulting most probable rupture force versus loading rate graph of the heparin/FGF-2 unbinding experiments, performed both in custom and commercial AFM. 44

Figure 4.10. Schematic of the experimental methodology for magnetically actuated bead attached cantilever and sample force curves for both a) specific interaction between streptavidin and biotin showing 285 pN rupture force, b) no adhesion/rupture event. 45

Figure 4.11. Loading rate vs. most probable rupture force obtained using piezo and magnetic cantilever actuation compared with the results of experiments obtained using a commercial AFM system. 46

Figure 4.12. Schematic representation of the dual actuation capability of the system and a sample force curve using heparin coated magnetic micropillars against FGF-2 coated cantilever (I-VI). Multiple single molecular events (R1-R2) are resolved clearly. 47

Figure 4.13. Most Probable rupture force versus loading rate graph for heparin/FGF-2 interaction performed in different days using new magnetic particle pulling technique with different size heparin labeled micropillars. 48

Figure 4.14. Schematic representation of the dual actuation capability of the system (0-V) and a sample force curve obtained during a biomolecular experiment. Multiple single molecular events (R1-R5) during phase 4 are resolved clearly. 49

Figure 4.15. a) Force histograms for biotin/streptavidin from magnetic bead pulling experiments b) Most probable rupture force versus loading rates for biotin/streptavidin interaction. 51

Figure 4.16. A sample force curve with 70 pN/s loading rate and showing 50 pN rupture force, from the biomolecular interaction between the heparin labeled magnetic bead and FGF-2 labeled cantilever. 52

Figure 4.17. Rupture force vs. loading rates graph for heparin and FGF-2 pulling experiments using magnetic bead actuation (black circles), piezo actuation (red stars) on the custom AFM setup and on a commercial AFM system (Dimension Edge, Bruker). 54

Figure 4.18. Probability of Rupture force for heparin and FGF-2 single molecular interaction and control experiments using magnetic bead pulling technique. 55

Figure 4.19. The most probable rupture force vs. loading rates graph for heparin and FGF-2 single molecular interaction. Each labels represents the experiments, which are carried out in different pH values of PBS solution using magnetic bead pulling technique. 56

Figure 4.20. A sample force clamp curve for heparin vs. FGF-2 interaction, obtained by applying a step magnetic force to the heparin labeled magnetic beads, without any feedback loop requirements. 58

LIST OF TABLES

Table 4.1. Bell's parameters for biotin/streptavidin interaction. 42

LIST OF SYMBOLS

f^*	Most probable rupture force
H_{AC}	Magnitude of alternative component of magnetic field
H_{DC}	Magnitude of direct component of magnetic field
k_B	Boltzmann's constant
k^o	Dissociation rate constant
M_{AC}	Magnitude of alternative component of magnetization
M_{DC}	Magnitude of direct magnetic component of magnetization
r_f	Loading rate
t	Time
T	Absolute temperature
T_{net}	Net torque
V	Volume
x_β	With parameter of energy landscape
ω	Angular frequency

LIST OF ACRONYMS/ABBREVIATIONS

2D	Two Dimensional
3D	Three Dimensional
AC	Alternative Current
AFM	Atomic Force Microscopy
BSA	Bovine Serum Albumin
CAD	Computer Aided Design
DAQ	Data Acquisition
DC	Direct Current
DI	Deionized
FEM	Finite Element Model
FGF	Fibroblast Growth Factor
GAG	Glycosaminogylon
IC	Integrated Circuit
MFM	Magnetic Force Microscope
PBS	Phosphate Buffered Saline
PCI	Peripheral Component Interconnect
pH	Power of Hydrogen
PID	Proportional-Integral-Differential
PSD	Power Spectral Density
PXI	PCI Extensions for Instrumentation
RMS	Root Mean Square
SLS	Selective Laser Sintering
TEC	Thermoelectric Cooler

1. INTRODUCTION

Atomic Force Microscopy (AFM) is a micro-scale cantilever based force sensing scientific apparatus for various applications in nanotechnology. It is widely used for surface topography imaging, material characterization, rheological measurements and measuring the interaction between biomolecules [1]. Conventional AFM systems can be classified in two major groups based on actuator configuration. A piezo-tube actuator either actuates the cantilever or the sample stage as shown in Figure 1.1. Both of these approaches have been implemented successfully by AFM researchers in academia and industry [2].

Although AFM is best known for high-resolution imaging, it has been used for three decades in the field of molecular biology and molecular biophysics as a versatile force measurement tool. A force resolution of a few pico-Newtons in liquid environments can be achieved via AFM technology at single-molecule level [2]. Application of biomolecular force spectroscopy technique successfully demonstrated the potential of the technology for various biomolecular measurements, such as antibody-antigen binding, receptor-ligand interaction, and protein folding/unfolding measurements at single-molecule levels [3-6].

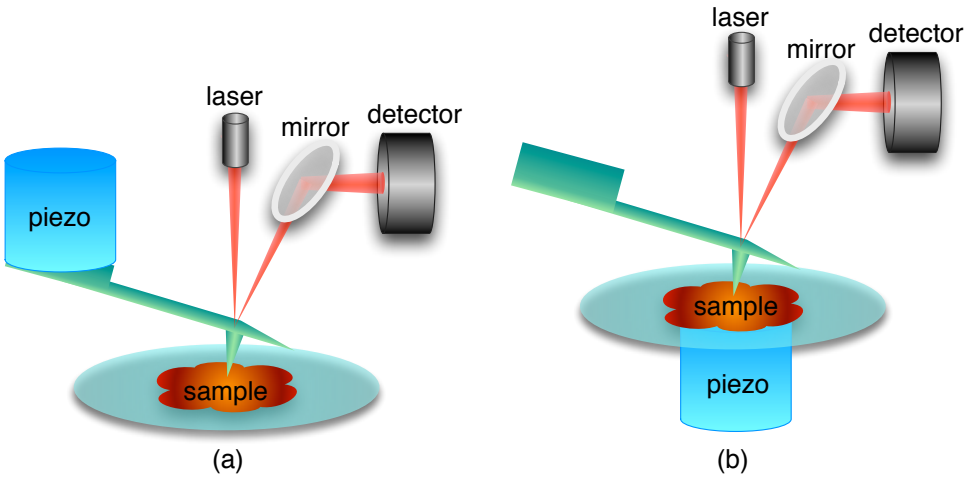

Figure 1.1. a) Cantilever actuated and b) sample stage actuated AFM system.

In the force spectroscopy technique, a cantilever is functionalized with a specific type of biomolecule. As a conventional method, the cantilever is actuated using a piezo-electric actuator over a sample surface that can also be functionalized with biomolecules. During the actuation, the cantilever comes recurrently in and out of contact with the sample surface. In the mean time, the deflection of the cantilever is detected using a readout laser. As seen in Figure 1.2, cantilever first comes in contact with the surface and applies a predetermined amount of force. Then the piezoactuator pulls the cantilever back until it comes out of contact. Due to the biomolecular interaction the cantilever bends negatively just before coming out of contact and the readout mechanism records a sudden jump corresponding the single molecular unbinding event. Using AFM technology, it is feasible to investigate the specific interactions between single pairs of biomolecules in aqueous environments. Quantitative studies on the structure, function and energy landscape of biomolecular interactions are applicable with the force spectroscopy technique [2].

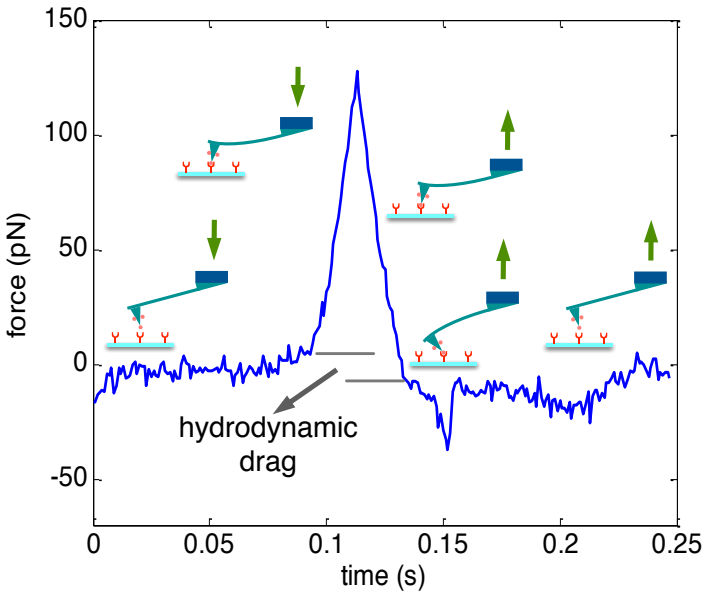

Figure 1.2. A sample force curve and cantilever deflection schematics from a single-molecule interactions.

It is necessary to load the biological bond between the molecular pair by actuating the cantilever with a wide range of speeds to perform some quantitative analysis on single biomolecular interactions. The unbinding forces between the biomolecules are related to the loading rate (hence actuation speed of cantilever). Therefore, having both stable actuators with minimized drift and fast actuators provides an advantage for low-speed and high-speed actuations, respectively.

Drift in the system induces spurious deflections on the cantilever especially at low actuation speeds, hence negatively affects the measurements. Mechanical instabilities and thermally induced deflection of the cantilever are the main sources of drift in the system. Deflection of the cantilever towards the substrate can harm the biological samples by increasing the contact forces on biomolecules [7, 8]. Furthermore, deflection of the cantilever due to drift leads to inaccurate force readings. Researchers have proposed different methods such as, using modified cantilevers, new probes [9-11], reference cantilevers [12, 13] and thermomechanicaly compensating microstages [7, 8] to overcome the effects of thermal drift problem in AFM. Large piezo actuation of the cantilever through its holder is one other main limitation for the actuation range since it disturbs the aqueous environment and cause drift in the system. Moreover, this may introduce additional modes into the complete mechanical system, and also limits the actuation capabilities at high speeds measurements [14].

The cantilever geometry also has a direct role on the limitation of the actuation speed considering the hydrodynamic drag effects [15, 16]. Actuating cantilevers directly, rather than actuating it through the holder is a partial solution of these problems. Several methods have been presented, such as magnetic actuation [17], photothermal actuation [18], acoustic pressure actuation [19] and capacitive actuation [20] to actuate the cantilevers directly. AFM head coupled with an electromagnet or a permanent magnet can be used to actuate magnetic cantilevers [21] or conventional cantilevers attached with magnetic particles [22].

Magnetic actuation capability can be added to a conventional AFM system by integrating an electromagnet and applying some mechanical modifications. Rapid prototyping techniques make it easy to construct customized AFM systems, since they

simplify the development of such setups according to user needs. A new AFM head for force spectroscopy applications was previously developed using selective laser sintering (SLS) [23]. The performance levels of the AFM system manufacturing with SLS was similar as compared to traditional manufacturing methods.

In this thesis, design and characterization of a new AFM setup having conventional piezoactuator together with an electromagnetic actuator and a novel AFM technique using miniaturized-magnetic particles as an actuator for biomolecular force spectroscopy and force clamp experiments are presented.

The AFM system is composed of basically two parts as AFM head and coil/sample holder. After completing the hardware design of the system the initial prototypes were manufactured from a rigid polymer using stereolithography technique (Rigid Opaque from Stratasys Ltd., MN, USA) to make required mechanical modifications easy. A PXI embedded controller (NI PXI-8102, National Instruments, TX, USA) programmed in NI-LabVIEW environment is used to drive the system in characterization and biomolecular experiments (see chapter 2).

After prototyping, characterization experiments are performed for AFM head and the electromagnetic actuator system both separate and together to demonstrate the performance levels (see chapter 3). Using a commercial AFM cantilever (SNL10-D triangular, Bruker probes), integrated noise level for AFM head is characterized as 2 pN in air, and 3 pN in water with a detection bandwidth of 1 kHz, which is adequate to measure the unbinding events between biomolecules. Performed Eigenfrequency analysis (using Comsol Multiphysics 4.3b) has a good agreement with the power spectral density measurements. On the electromagnetic actuator side, with a FeCo core, a flux density of over 0.55 Tesla is achieved at a working distance of 100 μm from the pole-piece, which is adequate to actuate the magnetic particles during the biomolecular experiments.

The temperature stabilization is extremely important for biomolecular experiments since temperature induced deflections on cantilever result in drift during the experiments. Experimental measurements shows with the water-cooling system and a Peltier cooler

(TEC), the temperature inside the experimental meniscus can be stabilized within 0.1° C after manufacturing the coil/sample holder from aluminum.

Single-molecule experiments have been conducted using the new AFM system. Different pairs of biomolecules are used to perform the force spectroscopy experiment using different techniques (see chapter 4). On one hand, the biomolecular interaction between biotin and streptavidin is investigated. These two proteins are a well-known ligand-receptor pair and have a wide literature background from the previous studies [24, 25]. Choosing biotin/streptavidin as a candidate pair is important for determination of the performance metrics and reliability of the new AFM setup and the novel methodology for single-force spectroscopy since the results of the experiment performed with biotin/streptavidin pair can be compared with the literature and improvements can be investigated. On the other hand, the heparin/fibroblast growth factor-2 (FGF-2) interaction is investigated. Heparin has been shown to interact with a large number of important proteins thereby regulating a range of biological activities including cell proliferation, inflammation, angiogenesis, viral infectivity and development. One of the most prominent examples of the Heparin-protein is that with the fibroblast growth factors, especially FGF-1 and FGF-2. FGF proteins are a kind of protein, which has a several effects on growth, differentiation, migration and survival of wide variety of cells [26, 27]. Both biomolecular pairs are probed using conventional techniques (i.e. piezoactuation or electromagnetic actuation) with both commercial and new custom AFM system. The results are in good agreement with each other and the literature.

After proving the results, a novel AFM technique with dual actuation capability is presented. In this new approach, the magnetic particles (i.e. microbeads, micropillars) are used as a secondary actuator together with the conventional piezoactuator. Using magnetic particles (i.e. magnetic beads) minimizes the size of the actuator down to a size comparable to that of a single molecule. Schematic representation of this new methodology with custom AFM system is shown in Figure 1.3. In this methodology cantilever used as a stationary force sensor is decorated with a specific type of biomolecule and probed with a counter-interacting molecule labelled to a magnetic particle.

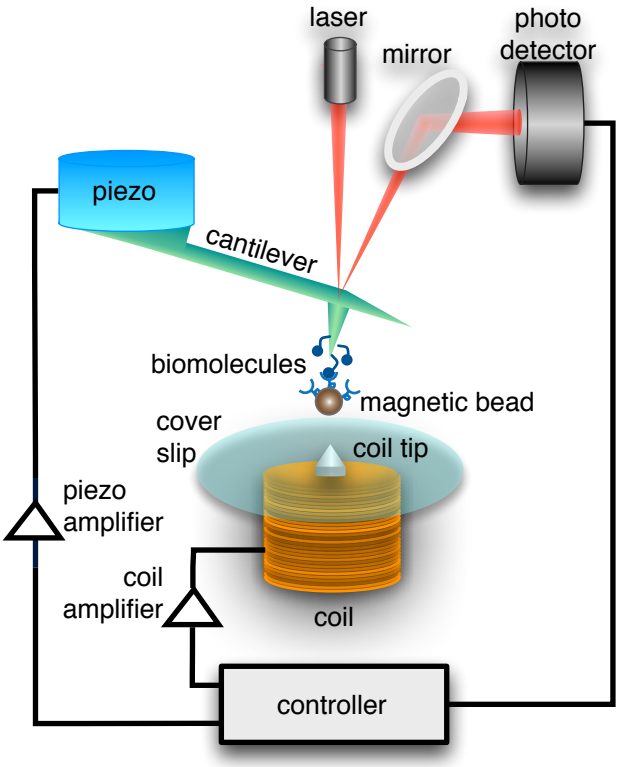

Figure 1.3. Schematic design of novel AFM system with bead actuation methodology.

It is possible to manipulate the magnetic bead without a substrate surface under the externally controlled magnetic field and field gradient. Manipulation tasks with objects varying in dimensions from nanometres to centimetres with five degrees-of-freedom with high resolution that is limited by imaging technology have already been demonstrated with electromagnetic manipulation setups [28]. The footprint of the magnetic actuator with a diameter of a few microns is orders of magnitude smaller than the commonly used piezotubes. The system dynamics is improved with miniaturized actuators, because the cantilever is kept stationary and the hydrodynamic drag forces on a magnetic bead actuated in viscous fluid is drastically smaller as compared to a conventional cantilever structure. The drag on a mechanical system is associated with damping and determines its thermal noise according to the fluctuation dissipation theorem. Reduced hydrodynamic drag improves force resolution and the stability of the system significantly. In addition, bead actuation technique substantially decreases the drift in the AFM measurements and also provides biomolecules from crushing, since the large mechanical loop between the

cantilever and the substrate is broken. Therefore, the introduced biomolecular measurement technique results in an increase of at least two orders of magnitude in loading rates and enlarges the bandwidth of the force spectroscopy applications. This is important to understand the dynamical behavior of biomolecules from a larger perspective.

In addition, magnetic particle actuation technique provides an inherited advantage on force clamp measurements. In conventional force clamp experiments a feedback loop is needed to keep the clamping force constant, since drift in the system cause the fluctuations in the clamping force due to the mechanical loop between the cantilever and the substrate. On the other hand, the force applied on magnetic beads is constant when the electromagnet is driven with a constant current signal. The current applied to the electromagnet determines the strength of the magnetic field, hence the force applied to the beads. Right after the functionalized cantilever grabs a magnetic bead, a constant clamping force is applied on the bead until a rupture event is observed. The duration of time between the instance when the force is applied and the instance of rupture, i.e. lifetime, is recorded.

2. DESIGN AND PROTOTYPE OF THE AFM SYSTEM

In this chapter the design and prototype of the new AFM system will be introduced. The AFM system was designed with a focus on increased hardware and software modularity especially for biomolecular applications. The modular design consists of an AFM head with a piezoactuator to actuate the cantilever through its holder, the electromagnetic actuation system including the coil and sample holder, and the control software to operate the system while recording input and output signals. Hardware design of the AFM system was built using a 3D CAD design software program (SolidWorks). A schematic of the AFM system with dual actuation capability both piezoelectric and electromagnetic together with the block diagram of the electronics and software is shown in Figure 2.1.

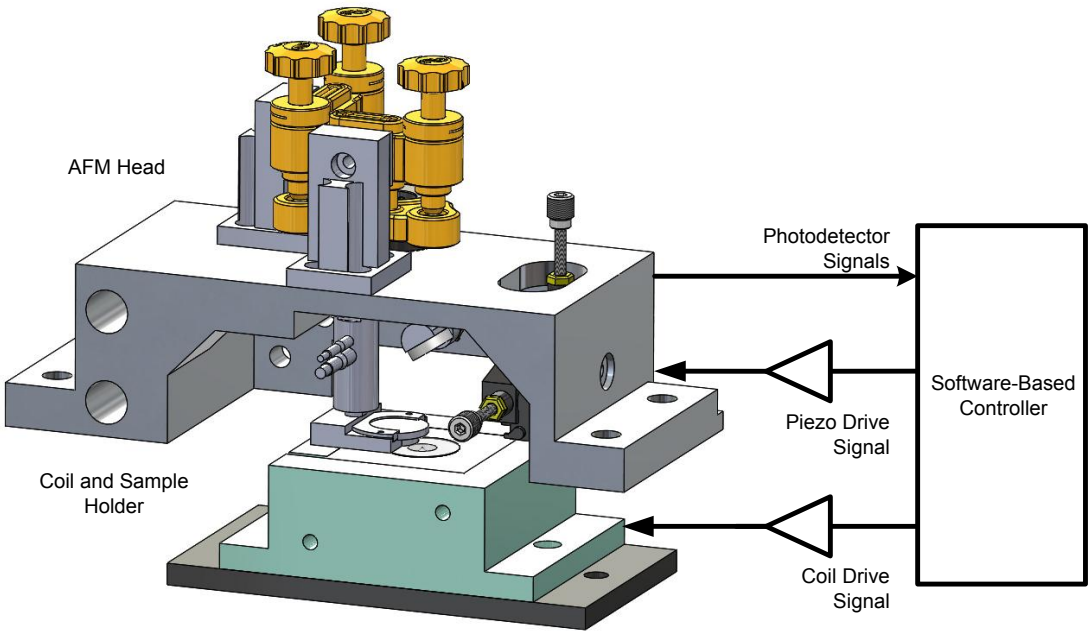

Figure 2.1. Schematic of the AFM system with dual actuation capability.

The prototypes for head and the sample/electromagnet holder are portable and were manufactured using low-cost jetting of a rigid polymer (Rigid Opaque from Stratasys Ltd., MN, USA). The electromagnet enables high-force DC and AC actuation of soft and hard magnetic cantilevers. The flexible software-based controller and the user interface were implemented in National Instrument's software environment, LabView, which runs on a Windows-based operation system. The software module can operate the AFM in force spectroscopy mode by driving the cantilever and monitoring the laser photodiode signals. It also provides the actuation signal for both the piezoactuator and the electromagnet. The dual actuation capabilities of the AFM allow for a wide range of biomolecular experiments.

2.1. Hardware Design and Prototype of the AFM Head

Hardware design of the AFM head was built using a 3D CAD design software program (SolidWorks). While designing the AFM head, it was very crucial to manage the design within the specifications, since one single head is wanted to be used for various kinds of single biomolecular applications. Front and side views of the AFM head are shown in Figure 2.2. The head is a compact design that fits in a space of 66.6 x 117 x 40 mm. The laser light source is mounted on top of the head using a kinematic rotational mount. This mount is connected to the head case by custom designed posts via M3 sized screws. The piezoactuator is mounted to the head case via a M5 screw. The free end of the piezoactuator carries to a customized cantilever holder that is specifically designed for force spectroscopy experiments allowing translational and rotational loading on the biomolecules. The cantilever is placed 60 mm away from the laser source. The reflected laser light from the cantilever is steered to the photodetector using a mirror with a diameter of 12 mm. The mirror is attached to an adjustment rotational knob. The distance from the mirror and the cantilever is 45 mm. The reflected light from the mirror falls on a quadrant photodetector. The position of the photodetector can be adjusted by a two-dimensional translational stage for the laser alignment on the detector.

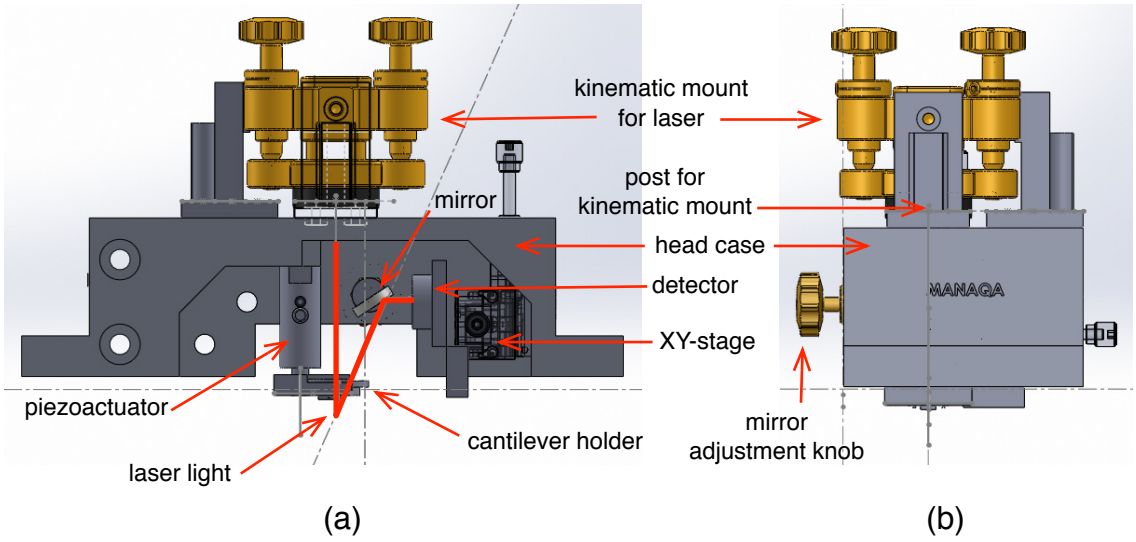

Figure 2.2. a) Front and b) side views of the AFM head.

Holder adapters were also designed to accommodate commercially available cantilever holders (air and liquid holders, Bruker Probes, CA, USA). Figure 2.3a shows the adapter for a liquid cell (DECAFMCH). The liquid cell is attached to the adapter via a custom clamp that is attached to the adapter via two M1 screws. The adapter dimensions are 22.95 x 25.75 x 6 mm. Figure 2.3b shows the other adapter for an in-air holder (DCHNM non-magnetic). The adapter has four nibs that register to the pins the holder. The designed adapter has dimensions of 19.5 x 15.75 x 3.8 mm and the length of a nib is 3 mm.

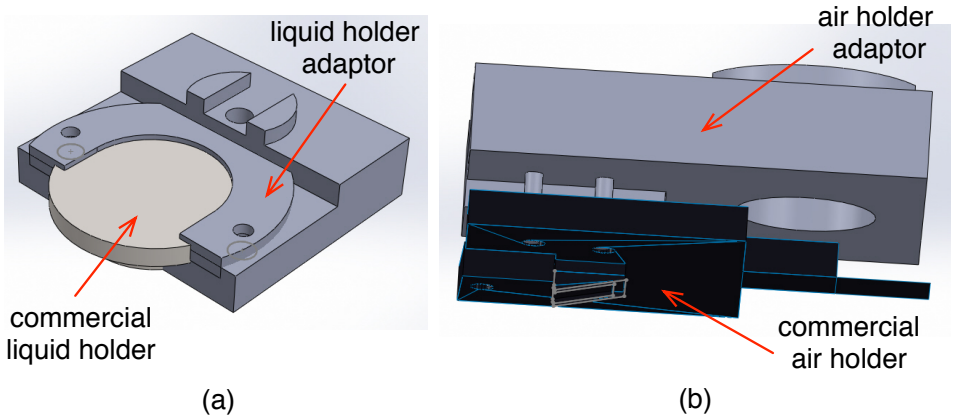

Figure 2.3. Custom adapters for commercially available a) in-liquid, b) in-air cantilever holders.

After completing the CAD design, a prototype was manufactured using a stereolithography process (Stratasys Objet Eden260V, MN, USA). The prototype was made of a general-purpose rigid resin material (Objet VeroWhitePlus, RGD835). The components of the head were assembled together as shown in Figure 2.4. Optical readout is realized using a red laser source (LPF-03, OzOptics, Ontario, Canada) at a wavelength of 633 nm. The fiber-coupled laser is connected to an aspheric focusing lens with a focal length of 13.9 mm. The predicted diameter of the laser spot at the cantilever is approximately 20 µm at a working distance of 60 mm. The laser is aligned on the cantilever using a rotational kinematic mount (SN100-F3K, Newport, CA, USA) that can be tilted up to 7°. Cantilever is actuated using a piezotube actuator (P-840.1, Physik Instrumente, Karlsruhe, Germany). The actuator is relatively short (32 mm in length, 12 mm in diameter) and covers a travel distance of 15 µm. This range is more than adequate for the force spectroscopy experiments and will be useful for the fine positioning the cantilever over the sample stage. The free end of the actuator will house commercially available cantilevers. Two adapters for commercially available holders (see Figure 2.3) were also manufactured for biomolecular force spectroscopy experiments.

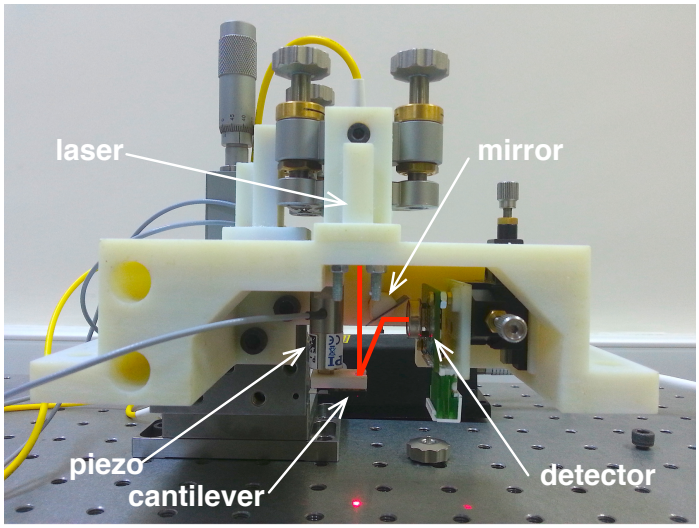

Figure 2.4. The assembled AFM head. Laser path is drawn for illustrative purposes.

A quadrant detector with integrated transimpedance amplifiers (QP50-6-18u-SD2, Pacific Sensor, CA, USA) is selected to measure the deflection of the cantilever. The amplifiers of the detector provide the vertical and horizontal difference signals together

with the sum signal. The responsivity of the photodetector cells is 0.4 A/W at 633 nm wavelength. A 2D translational stage with a travel range of 12.5 mm (T12XY miniature, Thorlabs, NJ, USA) is used to position the quadrant detector so that the returned laser beam will be aligned correctly.

2.2. Electromagnetic Actuator System Design and Prototype

Hardware design of the AFM body was built using a 3D CAD design software program (SolidWorks). The electromagnetic actuator system houses both the sample holder and the coil, and composes the AFM body. The AFM body is for pulling magnetic particles perpendicular to the cantilever plane. This configuration allows the pulling and force-clamp experiments with applied unidirectional force. A single coil is attached to the system with a holder as shown in Figure 2.5a. The holder and the coil are mounted on a movable stage that provides vertical position adjustment. Sample holder is a 0.2 mm-thick cover slip, mounted on a Peltier cooler (TEC) to control the temperature of the liquid during the bioexperiments. The TEC is a custom made one with a hole in the center so that the core of the coil gets through the TEC to make the tip to core distance minimum. In Figure 2.5b, there is a cross-sectional view of the coil holder. As it is seen there are a heat sink cup to circulate the cool water and an o-ring channel to seal the cooling system.

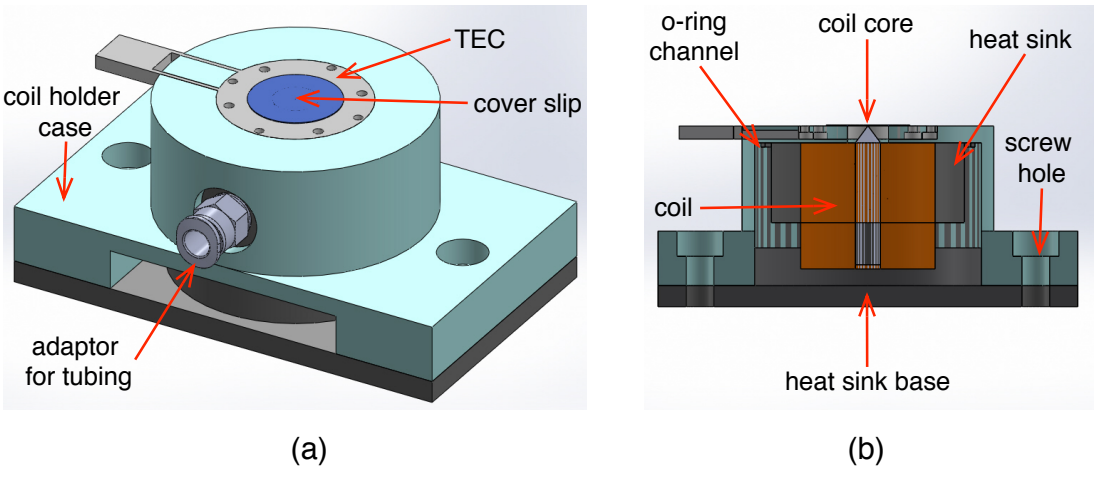

Figure 2.5. Designed AFM coil and sample holder for AFM body that allows applying translational force on magnetic micro-particles a) isometric view, b) Cross-sectional view.

After designing of coil and sample holder, a prototype was manufactured using a stereolithography process (Strasys Objet Eden260V, MN, USA). The prototype was made of a general-purpose rigid resin material (RGD525, yellow). The components of the AFM body were assembled together as shown in Figure 2.6. Around the coil there is a gap with water-cooling purpose. After manufacturing the holder from a nonmagnetic material, the water-cooling system and TEC can be used for temperature sensitive experiments.

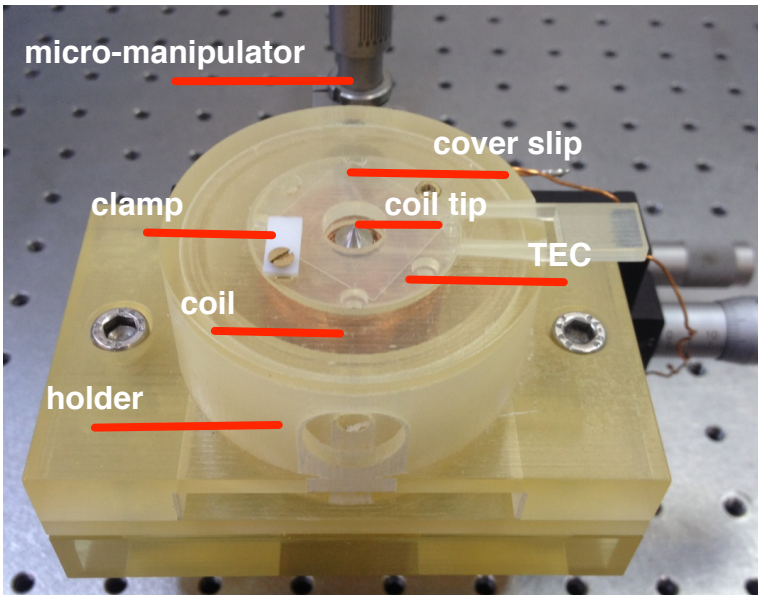

Figure 2.6. Assembled AFM body with sample holder surface and electromagnet.

2.3. Software-Electronic Design and User Interface

Block diagram of the electronics required for the AFM system is shown in Figure 2.7. The AFM system is controlled using a PXI embedded controller (NI PXI-8102, National Instruments, TX, USA) via The card has 8 analog inputs, 2 analog outputs and 24 digital inputs/outputs. The sampling rate of the card is 1.25MS/s, which is adequate for the biomolecular experiments. The controller is software programmed in NI-LabVIEW environment.

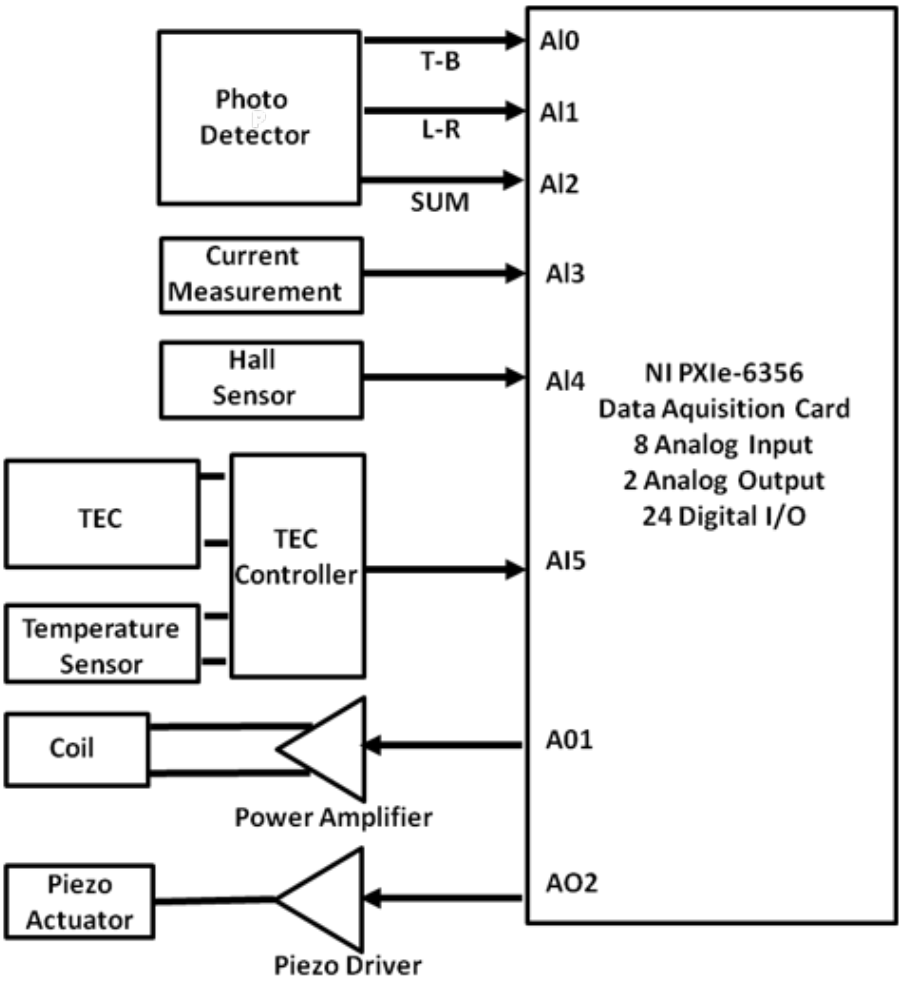

Figure 2.7. Block diagram of the electronics for the AFM system.

The left-right, bottom-top and sum voltage signals generated by the quadrant photodetector are fed to the DAQ card. Deflection of the cantilever is detected using these signals. The magnetic field generated by the coils is measured using proximity, i.e. Hall effect sensor (Melexis MLX90360, Belgium). The controller processes this information together with the cantilever position according to the needs of the experiment.

During operation, temperature of the coil may increase substantially. The temperature will be monitored continuously using a thermistor or an IC-based temperature sensor. The sensor is connected to a Peltier cooler (TEC) controller (TED200C, Thorlabs, NJ, USA) that keeps the temperature constant. The readout of the temperature sensor is also fed to the DAQ card.

A power amplifier (AE Techron 7224, IN, USA) is needed to drive the coil with large current and voltage drive signals. The power amplifier is connected to one of the analog outputs of the DAQ card. DAQ card will generate an arbitrary drive signal set by the software-based controller.

A piezo driver (Physik Instrumente E-610.0, Karlsruhe, Germany) is needed to operate the piezotube actuator. The piezo driver is connected to one of the analog outputs of the DAQ card. The sensor output of the piezo actuator can also be connected to an input channel of the DAQ card to monitor the position of the piezo actuator. DAQ card will also generate a digital control signal for the motorized stage. The position of the stage can also be monitored using the software.

The variable conversion requires a calibration routine implemented in the software. Deflection sensitivity of the cantilever, DS (µm/V), is obtained by pressing the cantilever on a hard surface using a triangular signal applied to the piezo amplifier. The user interface for the force spectroscopy and calibration sub-program is shown in Figure 2.8.

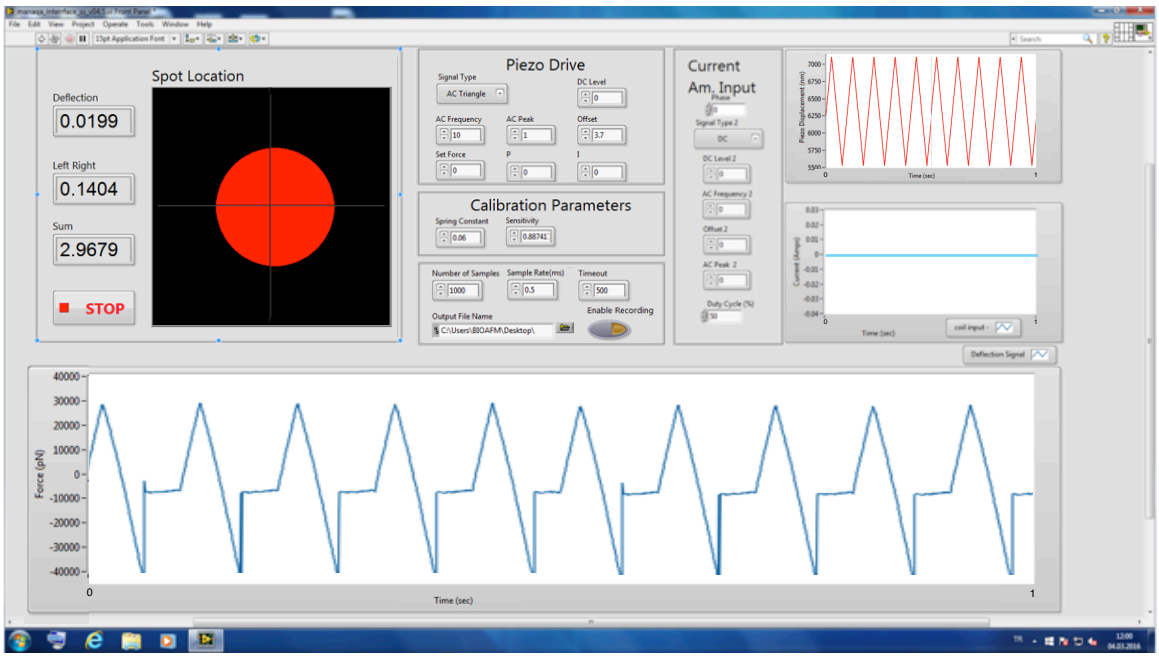

Figure 2.8. User interface VI for AFM system.

The spring constant of the cantilever, k (N/m), is obtained using thermal fluctuation method. In addition, the piezoelectric constant, D (μm/V), is provided by the manufacturer. Similar conversions are performed automatically. The interface is also capable of driving the piezo and coil amplifier at the same time for biomolecular pulling experiments both using piezo and magnetic actuations.

3. CHARACTERIZATION AND SYSTEM INTEGRATION

In this chapter characterization experiments and finite element model (FEM) analysis are presented for both custom design AFM head and the electromagnetic actuation system to investigate the performance levels of the new AFM setup. Moreover, the system integration phase of the custom AFM are demonstrated by coupling custom design AFM head manufacturing using stereolithography with the coil/sample holder machined from non-magnetic material. At the end of the phase, the integrated AFM system is ready for performing biomolecular experiments with temperature stabilization capability and minimized effects of drift.

3.1. Characterization of the AFM Head

Characterization of the AFM head basically involves the noise measurement of the AFM head both in air and liquid applications using commercially available AFM cantilevers. In addition to the experimental measurements, Eigenfrequency analysis of the AFM head is performed using a commercial FEM tool (Comsol Multiphysic 4.3b) to obtain a better understanding on the noise characteristic of the AFM head.

3.1.1. Noise Measurement of the AFM Head

A commercial cantilever (SNL10-D type triangular, Bruker Probes) was actuated with a constant speed against a silicon substrate using the piezo actuator in air during an experiment. By calculating the inverse slope of the contact portion of displacement (μm) versus deflection (V) graph, the deflection sensitivity was measured as 0.3678 μm/V for this specific experiment. The spring constant of the cantilever was calibrated using thermal fluctuation method. This method applies the energy equipartition theorem to find a relation between the Brownian motion of the cantilever and its spring constant. According to this

method, the kinetic energy of the cantilever due to the thermal vibrations is equated its potential energy by modeling the cantilever as an ideal spring [29, 30].

In Figure 3.1, Force time trace and the piezo actuation signal with respect to time are shown. The adhesion force was measured about 10 nN between the cantilever tip and silicon sample, in air. Minimum detectable force was calculated as 7 pN, by measuring the root mean square (RMS) value of deflection signal when the cantilever was out off contact with the surface.

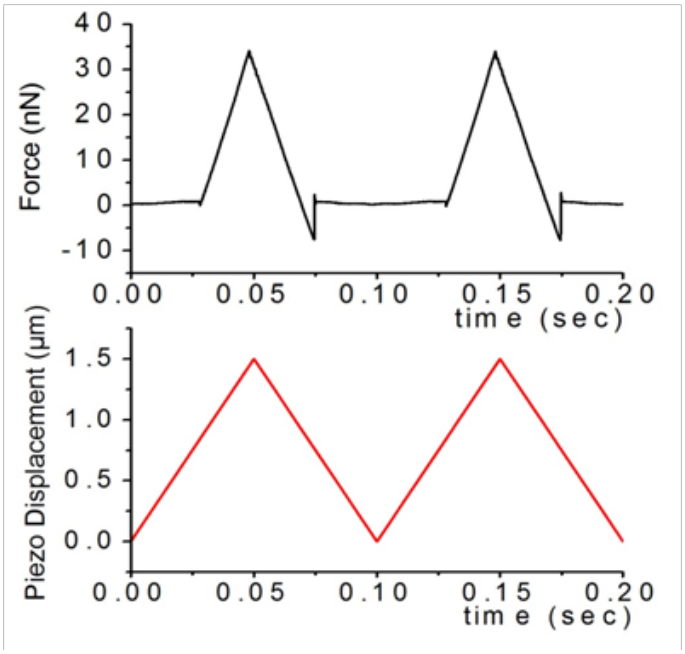

Figure 3.1. Force curve taken by actuating a silicon tip commercial cantilever (SNL10-D triangular, Bruker probes) using triangular piezo actuation over a silicon chip.

Figure 3.2 shows the power spectral density (PSD) of the same cantilever when it was out of contact with the substrate. Power spectral density can be obtained using the controller software described in chapter 2.3. The black curve corresponds to the PSD in air. As shown in the figure, the thermal peak of the cantilever is at 18 kHz due to the Brownian motion of the cantilever. The measured frequency is in agreement with the nominal resonance frequency of the cantilever (reported by the manufacturer between 12 and 24 kHz, SNL10-D, Bruker Probes). Integrated noise level in air applications is calculated as

1.8 pN, and in water 2.98 pN for 1 kHz bandwidth, which is adequate to measure the unbinding events between biomolecules. After immersing the cantilever in DI-water, the red curve was obtained. As it is expected, the thermal peak of the cantilever shifted towards the smaller frequencies due to the increased thermal mass and damping effect in DI-water.

There are several noise components in the AFM force spectroscopy applications: first, optical noise in the laser source due to the intensity fluctuations; second, electronic noise in the deflection sensor like photodiode shot noise and the Johnson noise of the preamplifiers; third, cantilever's mechanical noise coming from Brownian motion and the thermal drift; and forth noise induced by mechanical component and the acoustic ambient noise [31].

As a result of the noise measurement experiments, it is seen the noise level of the new AFM head is limited with the thermal noise of the cantilever, in liquid operations. Therefore, cantilever selection is very important for the force spectroscopy applications. By choosing the AFM cantilevers with different stiffness or geometry makes it possible to change the noise level limitation for this specific experiment in liquid.

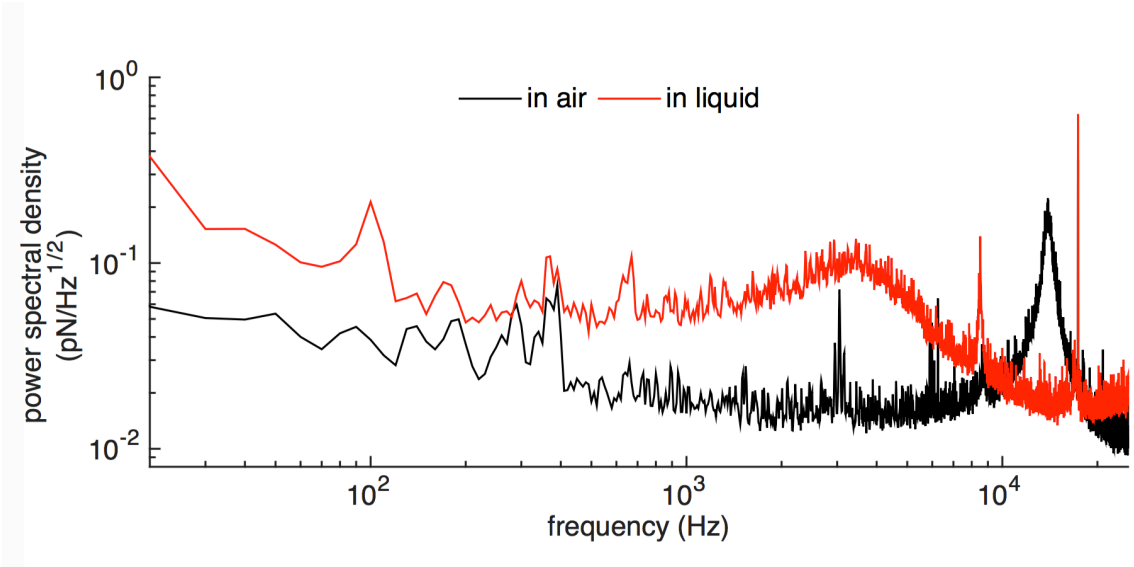

Figure 3.2. Power spectral density of a commercial cantilever (SNL10-D triangular, Bruker probes) in air (black curve) and in liquid (red curve).

3.1.2. Eigenfrequency Analysis with FEM

In this section, Eigenfrequency analysis of the modified AFM head is explained. The analysis was performed using Comsol Multiphysic 4.3b software for the assembled to demonstrate the Eigenfrequencies of the custom designed parts, which were manufactured using stereolithography. The commercial parts of the AFM head, such as microstages and kinematic mounts, were modeled as representative blocks on the FEM simulations.

In Figure 3.3, meshed 3D FEM model of assembled AFM head is shown. As it is seen, the kinematic mount for laser and the microstage for photodetector were modeled as representative blocks to introduce corresponding load and mass in the model. Apart from the commercial parts such as, representative blocks for micro-positioners, piezo, liquid cell and the photodetector, all other parts are manufactured using a rigid polymer using stereolithography. By introducing specific joint conditions between the parts in the assembly and assigning the material properties to the parts, the final FEM analysis was simulated. Since there are infinitely many mode shapes for the modified AFM head assembly, the frequency range of detection was considered for the solution.

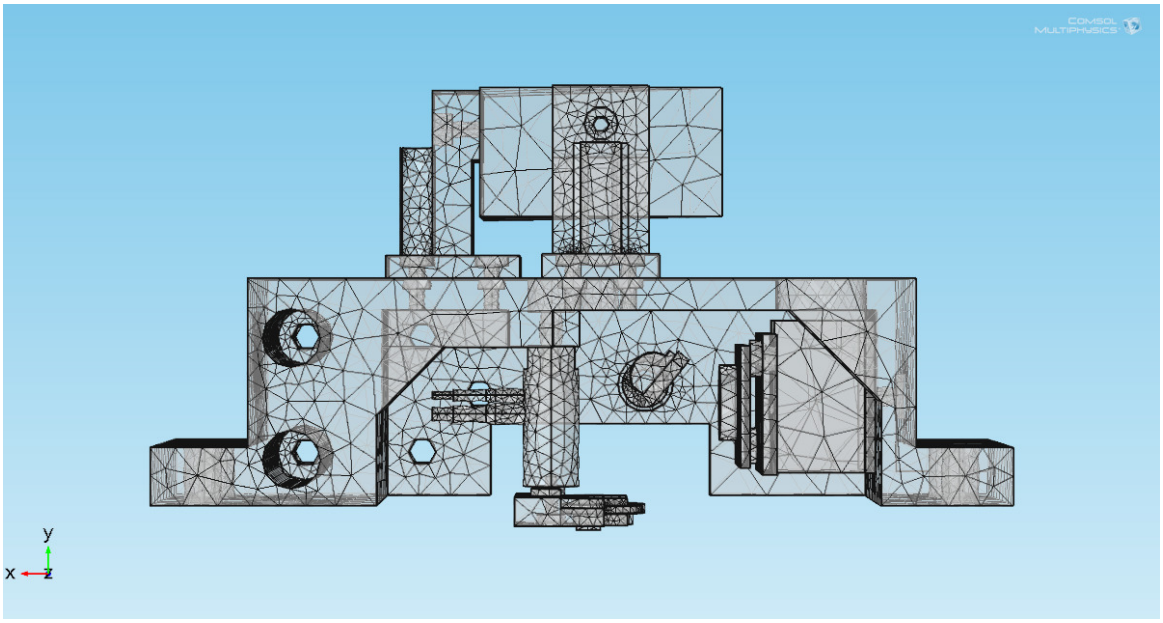

Figure 3.3. Meshed AFM head assembly using Comsol Multiphysic 4.3b

To begin with, in order to compare the result of FEM simulation with the realistic case, a power density spectrum (PDS) measurement was made on a commercial cantilever (SNL10-D triangular, Bruker Probes). As seen in Figure 3.2, the cantilever has a thermal peak around 18 kHz due to the Brownian motions in air. However, there is another mechanical peak around 3 kHz.

The result of FEM simulations performed to identify that unknown peak in the power spectrum of the cantilever indicates a peak around 3 kHz. Figure 3.4 shows the result of the FEM simulations for one specific Eigenmode around interested frequency. As it is seen, there is a mode shape at the 3.3 kHz for the custom adaptor part, which combines the commercial liquid cell to the piezoactuator. As a result of the FEM simulation, the source of the unknown peak in PDS is found that as an Eigen mode of the liquid holder adaptor, which is manufactured from a rigid polymer using sterolithography. By comparing the PDS results with FEM analysis, the source of the mechanical peak in air around 3 kHz came to light.

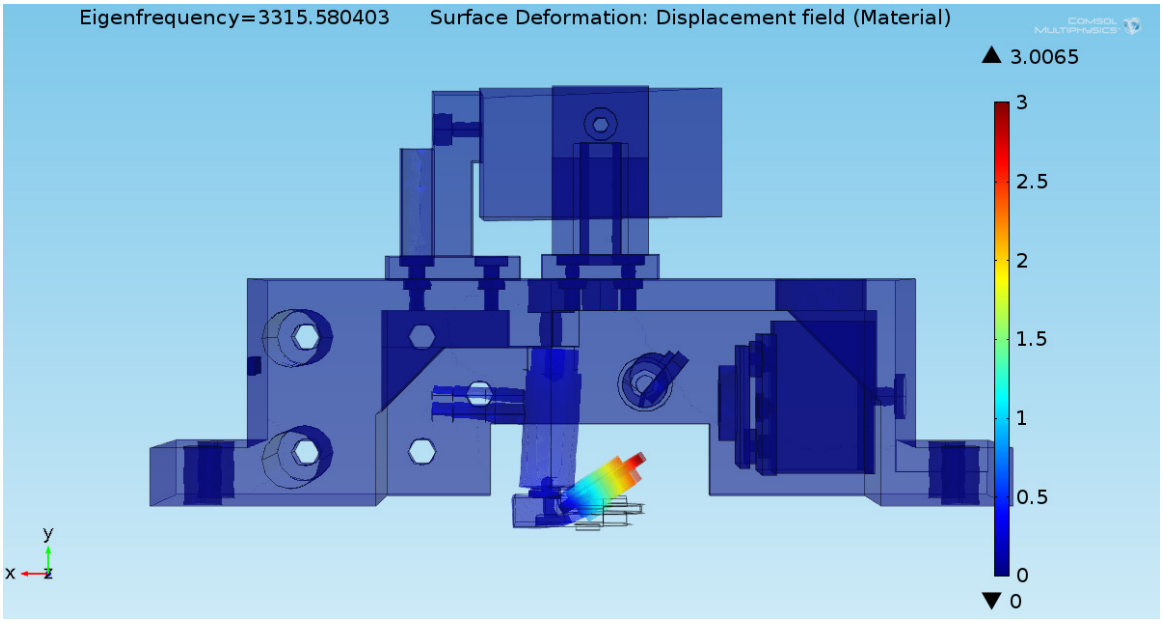

Figure 3.4. Result of FEM simulations for specific Eigenmode in the AFM head.

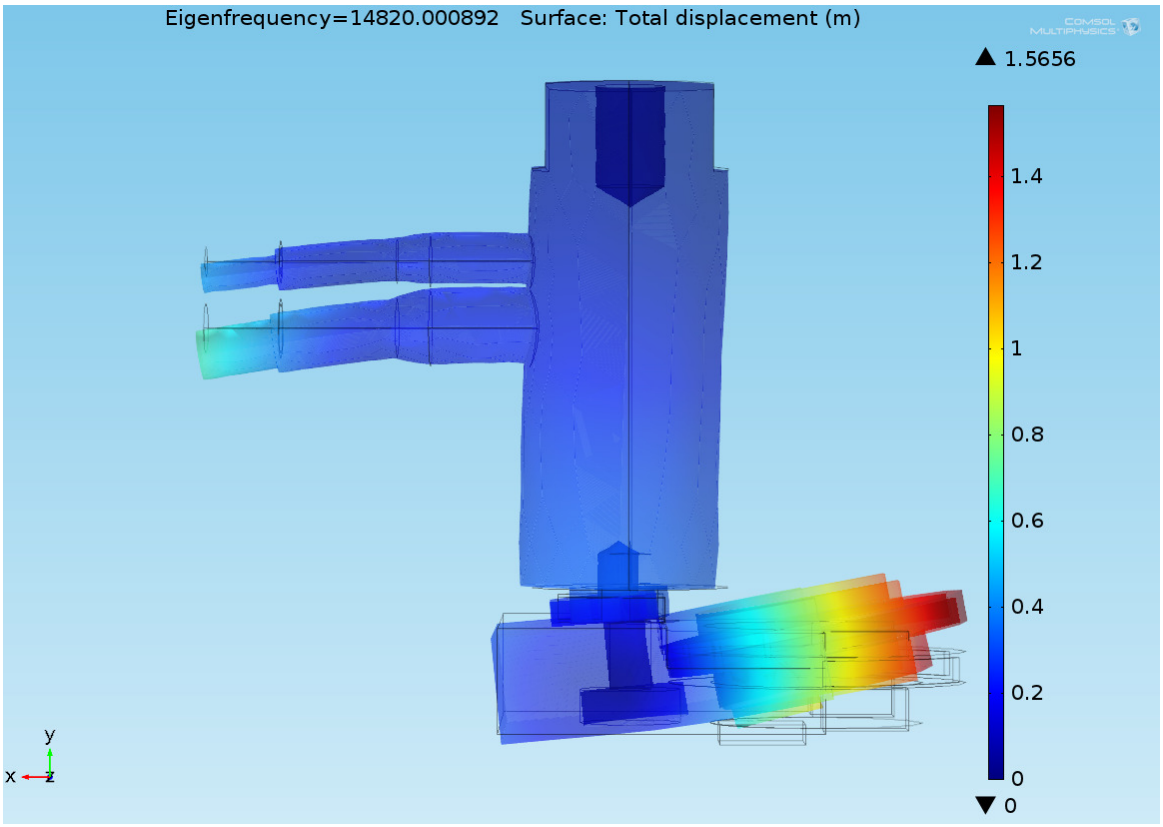

Figure 3.5. FEM Eigen frequency analysis for a glass ceramic adaptor.

Since the FEM analysis and the PSD measurements results were consistent, the FEM model was justified. After this step, the material dependence of this mode shape is investigated. In a new FEM model the material of the adaptor is switched to glass ceramic, which is a machinable ceramic type. Since the stiffness of the glass ceramic is bigger than the stiffness of the polymer that was used in prototyping of custom designed AFM parts, it is expected that the mode shape of the liquid holder adaptor shifts towards the higher frequencies.

The result of the FEM analysis can be seen in Figure 3.5. As it is expected using a more stiff material like glass ceramic we can push the mechanical peak coming from the liquid holder adaptor to higher frequencies. For the case of the glass ceramic the Eigenfrequency of this mode will be around 15 kHz, which is five times larger than the present case.

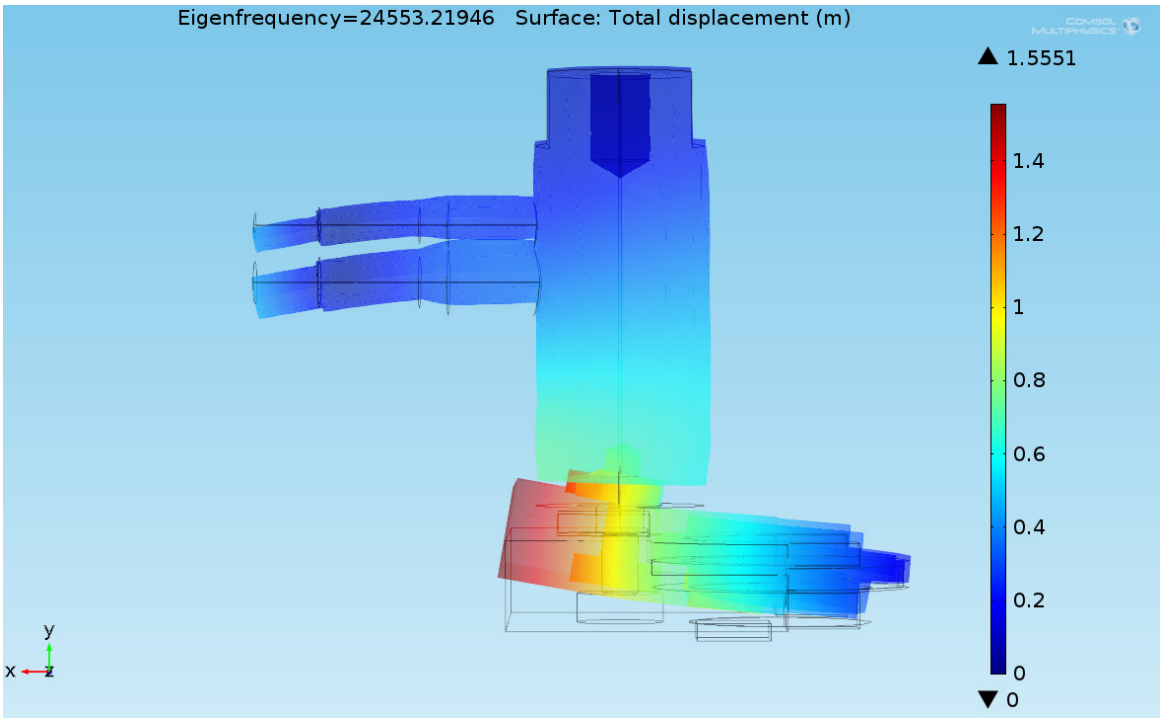

Figure 3.6. FEM Eigen Frequency Analysis for a structural steel adaptor.

If same analysis is performed for a structural steel, which has a higher elastic modulus we can push the peak even further. Figure 3.6, FEM simulation shows an Eigenmode around the 25 kHz. According to this FEM simulation even the commercial piezoactuator has a mode shape and deformation around that point.

3.2. Characterization of the Electromagnetic Actuator System

Characterization of the electromagnetic actuator system involves the magnetic characterization measurements for both AFM head and electromagnetic actuator. In this section performance levels of the coil and the behavior of the AFM head under magnetic field are demonstrated. First the electromagnet is characterized using Hall effect sensor. Then, AFM head is characterized under the magnetic field using commercial magnetic force spectroscopy (MFM) cantilevers and soft magnetic particle attached cantilevers.

3.2.1. Magnetic Characterization of the AFM Head and the Electromagnatic Actuator System

The DC magnetic field generation capability of the electromagnet was quantitatively characterized with a micro-hall sensor (Nanomagnetics Ltd, Ankara, Turkey) having an active sensing area of 1x1 μm^2 as seen in Figure 3.7a. The magnetic flux density was measured at various input current densities. The axial decay of the flux density from the tip of the electromagnet was found to be an excellent match with the FEM design simulations performed to investigate the change in the magnetic flux density with the distance from the tip, shown in Figure 3.7b. A flux density of over 0.55 Tesla is achieved at a working distance of 100 µm from the pole-piece. Which is adequate to perform experiments using electromagnetic actuations.

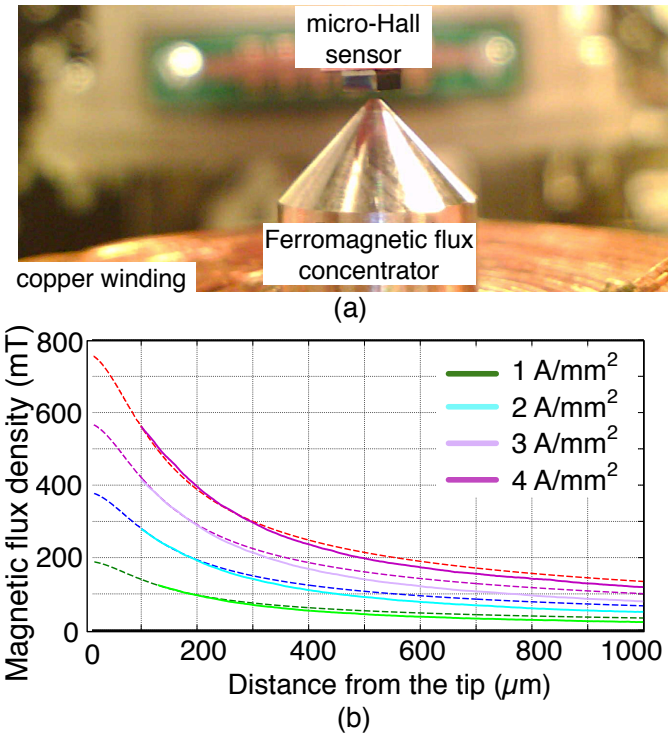

Figure 3.7. a) The electromagnet is shown along with the micro-hall sensor which was used for characterizing the magnetic flux density. b) The experimentally measured vertical magnetic flux density is compared with FEM simulations at various current densities.

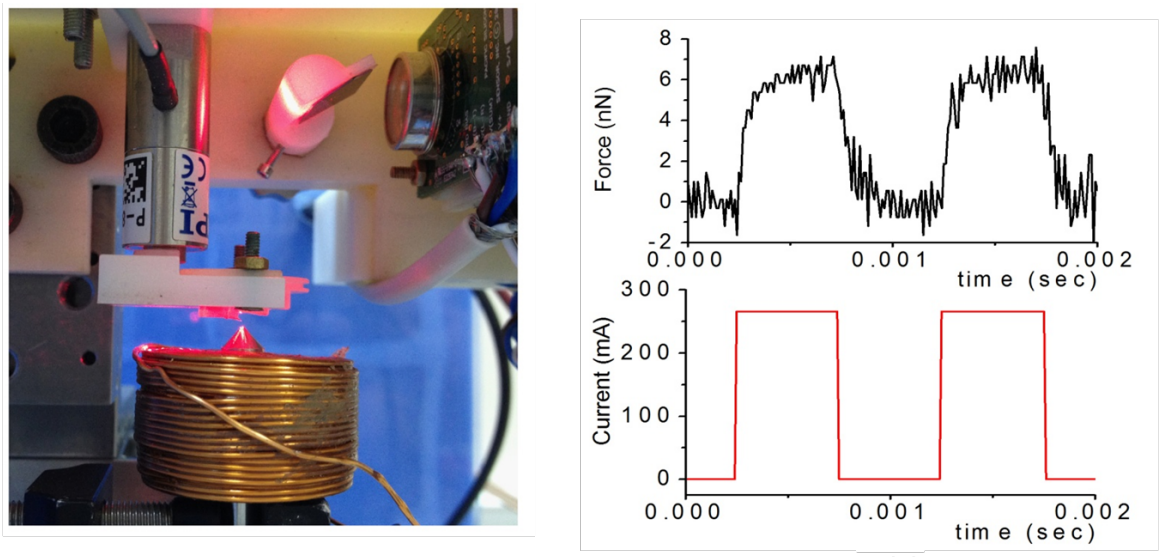

Figure 3.8. a) An electromagnet is placed under the AFM to see the magnetic actuation effects. b) Magnetic actuation of a commercial MFM cantilever (MESP, rectangular, Bruker Probes) in air with a square signal, having an amplitude of 300 mA at 1 kHz.

After the characterization with micro-hall sensor, this electromagnet was placed under the custom AFM head as shown in Figure 3.8a. To be able to actuate the cantilever with magnetic force, a commercial MFM cantilever (MESP, rectangular, Bruker Probes) was placed on the cantilever holder. The cantilever is made from a hard magnetic material and its nominal stiffness value is 2.8 N/m. The electromagnet was driven with square signal up to 5 kHz. In Figure 3.8b, 1 kHz magnetic actuation of a commercial MFM cantilever in air is shown. At 1 kHz, a square signal with 300 mA amplitude results almost 7.5 nN magnetic force over the MFM cantilever.

After the hard magnetic material MFM cantilever actuation, the result of a soft magnetic material actuation was tested with a magnetic cobalt-nickel alloy micropillar, having a diameter of 1.5 µm and a length of 10 µm. The micropillar was attached to a tipless cantilever (CSC38, tipless rectangular, Bruker Probes) as shown in Figure 3.9a. The electromagnet was actuated with a sinusoidal signal at 500 Hz. In Figure 3.9b, the current input does not have any offset. The mean of the sine input is zero. As a result, the output force signal has twice the frequency as compared with the input signal. On the other hand,

the force on the cantilever has the same frequency with the actuation signal when the offset of the signal is a nonzero, as seen in Figure 3.9c. Due to the soft magnetic property of the micropillar, the mechanical actuation frequency doubles for a periodic actuation signal having zero mean value.

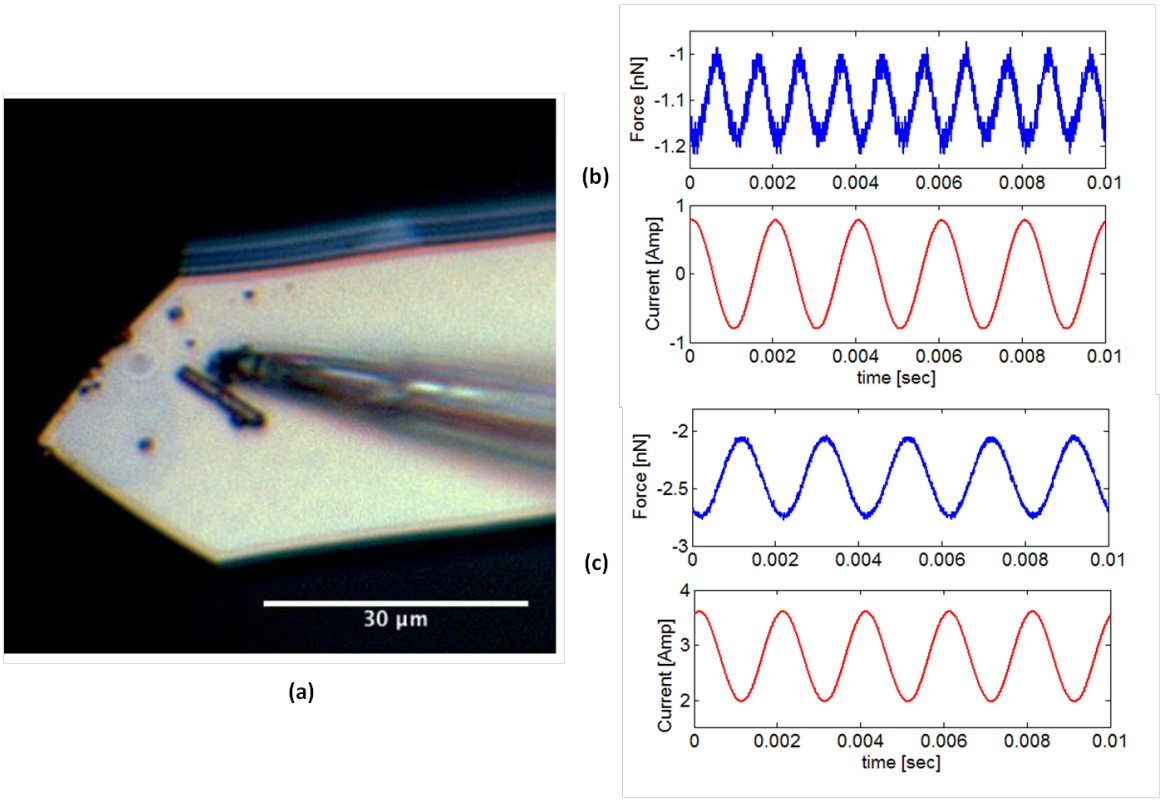

Figure 3.9. a) The picture of a soft magnetic micropillar, attached to a tipless AFM cantilever (CSC38-Tipless, Bruker Probes). Magnetic actuation of the micropillar attached cantilever b) with a zero mean sinusoidal input c) with a positive mean sinusoidal input.

The following equations show that an AC signal without a proper DC level results in a mechanical actuation at twice the actuation frequency [32]. The net torque, T_{net} on a magnetic material resulted from a sinusoid driving current can be written as in Eq.3.1 where V is the volume of material, M_{DC} and M_{AC} are magnitudes of magnetization, respectively DC and AC components, H_{DC} and H_{AC} are magnitudes of magnetic field, respectively DC and AC components, ω is the angular frequency and t is time. Assuming there is not any net torque from the dc component, Eq. 3.1 simplifies to Eq. 3.2, which is

equivalent to Eq. 3.3. In addition changing the direction of current has no effect on the direction of net torque, since the sign of $M_{AC}H_{AC}$ product is always positive.

$$T_{net} = V(M_{DC} + M_{AC}\sin(\omega t))(H_{DC} + H_{AC}\sin(\omega t)) \tag{3.1}$$

$$T_{net} = V(M_{AC}\sin(\omega t))(H_{AC}\sin(\omega t)) \tag{3.2}$$

$$T_{net} = {}^{V}/_{2}\, M_{AC}H_{AC}(1 - \cos(2\omega t)) \tag{3.3}$$

The AC actuation forces of the electromagnet with FeCo core were characterized using a commercial MFM cantilever (MESP, rectangular, Bruker Probes). The cantilever was placed on the cantilever holder in air medium. Furthermore, the electromagnet was located under the AFM head as shown in Figure 3.8a. The Si cantilever has a hard magnetic CoCr coating and its stiffness was calibrated as 1.12 N/m using thermal fluctuation method as explained in chapter 3.1.1. To begin with, the electromagnet was driven with a square wave up to 10 kHz. In Figure 3.10a and Figure 3.10b, 10 Hz and 1 kHz magnetic actuation of a commercial MFM cantilever in air using square actuation signals are shown, respectively. At 1 kHz, a square wave with 300 mA amplitude results in a magnetic force of 7.5 nN on the commercial MFM cantilever.

The frequency response for the measured current on the coil and the force measured on the cantilever is plotted in Figure 3.10c. In order to obtain these frequency responses, coil was driven using sinusoidal input signals having same amplitudes but various frequencies ranging from 1 Hz to 10 kHz. The current was measured by reading the voltage drop over a small resistance (68 ohm) placed at the input of the coil. Moreover, the force response was measured directly from the photodetector output using the same commercial MFM cantilever as in the square magnetic actuation measurements. According to the results of these measurements, the force response, which has a cutoff frequency around 1 kHz, decays faster than the current response with a cutoff frequency around 3 kHz. The reason behind that situation is the lowering of effective permeability due to

hysteretic and eddy current losses in the core material. The bandwidth of the force response can be significantly increased using the ferrite core, which has lower hysteretic and eddy current losses, albeit at the cost of overall reduced force, because of its lower saturation induction (Ms ~ 0.4T).

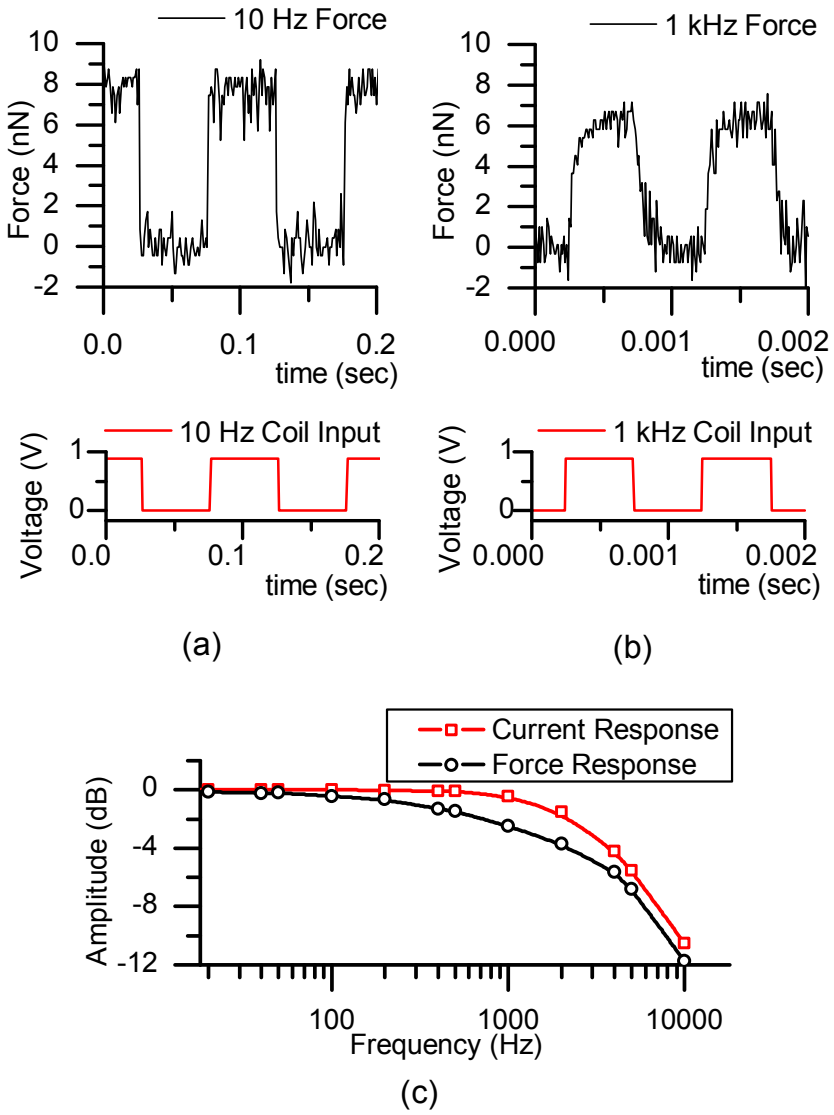

Figure 3.10. Magnetic actuation of a commercial MFM cantilever (MESP, Bruker Probes) in air a) at 10 Hz and b) at 1 kHz using rectangular voltage drive signals. c) Force and current response graph with respect to frequency.

3.3. System Integration

After the characterization experiments and simulations for the AFM head and electromagnets, the AFM head was integrated with the pulling electromagnet to carry out the system integration characterizations and the magnetic actuation experiments. The AFM hardware assembly is placed on a vibration isolation table and an acoustic enclosure for minimal noise operation, as shown in Figure 3.11a. The dual actuation capabilities of the AFM allow for a wide range of biomolecular experiments.

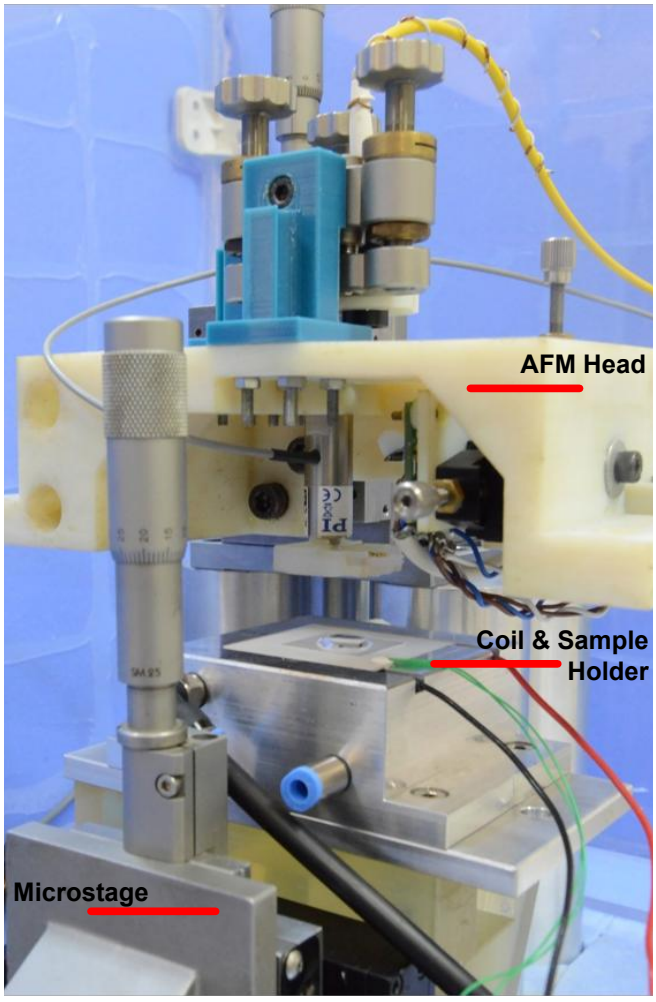

(a)

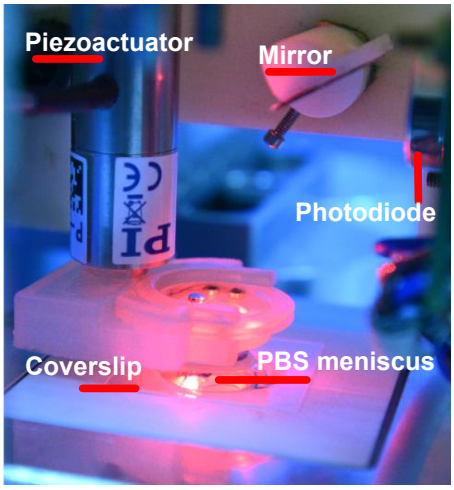

(b)

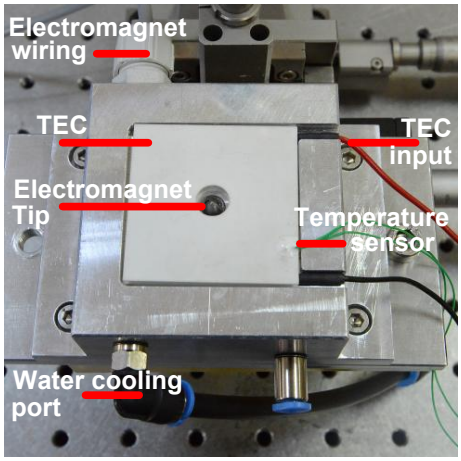

(c)

Figure 3.11. a) Integrated AFM head with coil-sample holder, b) the manufactured AFM head with commercial elements, c) coil-sample holder.

The 3D-printed AFM head shown in Figure 3.11b comprises of a fiber-pigtailed laser diode (λ=650nm, Oz Optics Ltd. Ottowa, Canada), which focuses the light beam onto the cantilever mounted on a piezoactuator (P-841.1, Physik Instrumente GmbH). The reflected light is directed by a mirror into a quad-photodiode array (Pacific Silicon Sensor, CA, USA). The cantilever is mounted to a commercially available liquid cell (DECAFMCH-PFT, Bruker, USA), which is attached to the piezoactuator via a 3D-printed custom adaptor. The piezoactuator has a vertical range of 15 microns. A kinematic optical mount (Newport Corporation, CA, USA) embeds the laser fiber and is used to orient and focus the laser beam onto the cantilever. The mirror directing the laser beam has a rotational degree of freedom and the photodetector is mounted on a miniature two-axis translator (Thorlabs Inc. NJ, USA). The AFM head has been designed to allow easy integration onto an electromagnetic coil system for direct cantilever actuation, in addition to other magnetic applications.

Figure 3.11c shows the coil-sample holder. The electromagnet consists of an optimized ferromagnetic core geometry and copper winding. The design objective was to maximize the force on a magnetic film-coated or magnetic particle-attached cantilever at a working distance of 100-150 μm from the pole-piece of the electromagnet. The exchangeable core-piece is made of FeCo alloy (Vacoflux50^{TM}) because of its high magnetization saturation (M_s = 2.35T), which corresponds to higher actuation force. Since biomolecular experiments have strict requirements on temperature control and stability, we implemented a dual cooling stage comprising a thermoelectric cooler (UEPT-440-127-079E120 – Uwe Electronic GmbH) for fine-regulation of temperature on top of a water-based cooling system.

Figure 3.11 shows the final version of the integrated AFM head. In order to use the TEC and water-cooling system effectively, the coil holder machined from non-magnetic aluminum. All the magnetic actuation based biomolecular experiments (see chapter 4) were performed on this final system.

3.3.1. Temperature Control in Liquid Operation

Biomolecular interactions are extremely sensitive to environmental temperature and fluctuations. Thermal drift induces cantilever deflection and changes the zero-force level, which are detrimental for force spectroscopy. Joule heating due to the current running through the electromagnet can perturb the experiments. A temperature control system, which can regulate the temperature fluctuations from the electromagnet operation in the fluid environment to within 0.1° C, was developed. The control was achieved using sub-mm sized thermistor (Pt-100, with accuracy 0.03° C [33]) placed in the liquid meniscus along with a thermoelectric cooler and a closed-loop temperature controller (12 mW temperature controller, ThorLabs). With the adjustment of P, I and D share of the control loop, settling time and over-shooting are minimized to have a fast and stable temperature control.

Figure 3.12 shows how the temperature of a cantilever rises when the electromagnet is turned on with the initial temperature of the cantilever was 25.9 °C. The electromagnet was driven with a square wave with a frequency of 0.2 Hz and peak current of 1.8 A for 100 min. The temperature increased to a temperature of 32.5 °C when the temperature controller was turned on at t=53 min.

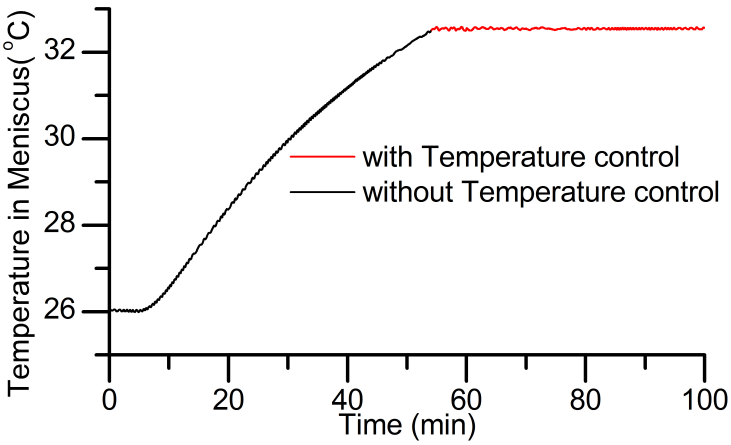

Figure 3.12. Temperature trace of an immersed cantilever actuated using the electromagnet. The temperature starts rising when the electromagnet is turned on at t=5 min. The temperature controller is turned on at t=53 min to stabilize the temperature.

3.3.2. Improvement in Drift Problem in AFM Measurements

The new system and the magnetic actuation methodology together eliminate the need of the interaction between the cantilever and a sample surface during the experiments (see chapter 4.3 and chapter 4.4). The capability of performing experiments away from the sample surface is advantageous since the large mechanical loop between the cantilever and the sample surface is broken. The mechanical loop is a significant source of drift in conventional AFM setups. In addition, keeping the cantilever away from the sample surface improves its dynamics by eliminating the hydrodynamic wall effect.

A long time scale drift experiments were performed using new AFM system in comparison with a commercial AFM system (Dimension Edge, Bruker). A commercial cantilever (MLCT-C type, V-shaped Silicon Nitride cantilever, Bruker) was actuated in and out off contact with a coverslip using the piezoactuator of the commercial system to characterize drift in the setup. For this purpose, a square wave signal with constant amplitude was applied to the piezoactuator and monitored the deflection of the cantilever. Figure 3.13 (black line) shows the contact force on the cantilever was doubled during duration of 500 s. Apparently, the distance between the base of the cantilever and the sample surface decreased due to the drift in the system. This resulted in an increase in the contact force. Increase in the contact force is detrimental especially when the tip of the cantilever is functionalized with biomolecules as they can be harmed.

A similar experiment was repeated with the new AFM setup. A ferromagnetic magnetic bead with a diameter of 30 μm was glued on a same type of cantilever. The bead-attached cantilever was actuated by applying a square wave signal with constant amplitude to the electromagnet while observing the deflection. The red line in Figure 3.13 shows the deflection of the cantilever due to the magnetic actuation. The amplitude of deflection signal keeps constant during the entire experiment. The mean value of the deflection signal decreases with respect to time due to the temperature response of the cantilever.

As it is seen, the differential amplitude of the force on the cantilever is quite stable. This new AFM technique not only eliminates the drift effects from the measurements but

also prevent the biomolecules from crashing due to the thermally induced forces on cantilever, by avoiding a rigid mechanical loop between the cantilever and the substrate, which are magnetic particles (see chapter 4.3 and chapter 4.4).

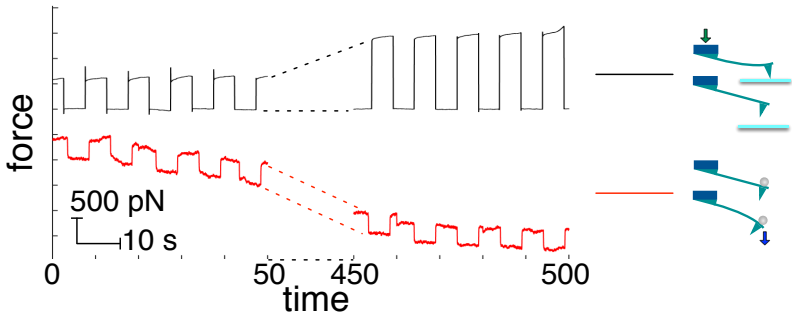

Figure 3.13. Time traces for the characterization of long time scale drift obtained using a commercial AFM (black) and magnetic actuation of a bead-attached cantilever (red).

4. BIOMOLECULAR EXPERIMENTS

To fully understand the role of biomolecular interactions and to explore its energy landscape, it is necessary to investigate the dynamic response of individual biomolecular pairs under external mechanical forces. According to the Bell model, the application of pulling force reduces the activation energy barrier of biomolecular interaction toward dissociation. Therefore, the lifetime of the complex reduces [34, 35]. Moreover, the rupture force between the biomolecular pairs should increase with the increasing rate of force application [25].

The Bell model predicts a linear relationship between the most probable rupture force, f^* and logarithm of the loading rate, r_f. The loading rate is the rate of fore application while the bond between the biomolecules is loaded and depends on cantilever stiffness, actuation speeds and also the extension of the biomolecular bond. The nominal loading rate can be calculated by multiplying the cantilever stiffness with actuation speeds, whereas the actual loading rate is the slope of the force curve before the rupture occurs (see Figure 4.1). According to Bell, the dissociation rate of a bond is amplified by the application of an external force. Bell's parameters, i.e. the dissociation rate constant, k^o which corresponds the dissociation rate at the absence of external force and width parameters of energy landscape, x_β which is a parameter that characterizes the relationship between the external force and dissociation rate are extracted from the loading rate versus most probable rupture force information using Eq. 4.1, where k_B is the Boltzmann's constant and T is the absolute temperature [25].

$$f^* = k_B T/x_\beta \ln\left(x_\beta/k^0 k_B T\right) + k_B T/x_\beta \ln\left(r_f\right) \tag{4.1}$$

In this chapter, the various methodologies for single molecular experiments using AFM systems and single molecular force spectroscopy results are presented. Two various biomolecule pairs were selected as a candidate to perform the force spectroscopy

experiment using different techniques. As a first candidate, the biomolecular interaction between biotin and streptavidin pair was investigated. Biotin and streptavidin are two proteins, which have the strongest protein-protein bond in the literature [25].

Heparin/fibroblast growth factor-2 (FGF-2) interaction was selected as a second candidate. Heparin is a sulfated polysaccharides belonging to glycosaminoglycan (GAG) family. Heparin is only product by mast cells. It functions as an anticoagulant, and extensively used in medical practice. It plays an important role in fundamental biological process by binding to proteins. Over the last 20 years, Heparin has been shown to interact with a large number of important proteins thereby regulating a range of biological activities including cell proliferation, inflammation, angiogenesis, viral infectivity and development. One of the most prominent examples of the Heparin-protein is that with the fibroblast growth factors, especially FGF-1 and FGF-2. FGF proteins are a kind of protein, which has a several effects on growth, differentiation, migration and survival of wide variety of cells [26, 27].

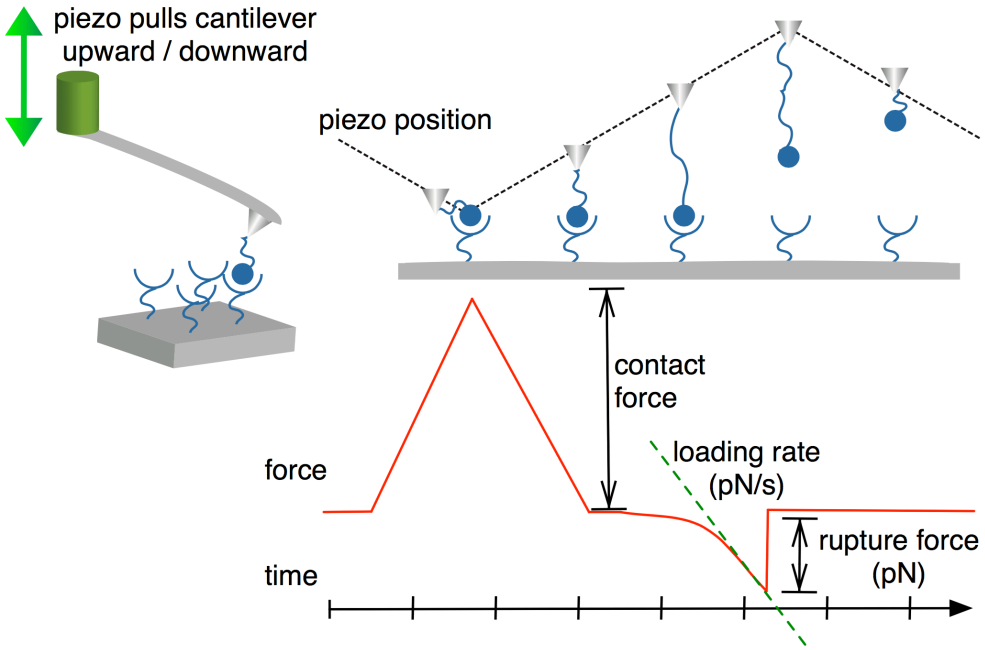

Figure 4.1. Schematics of biomolecular pulling experiment with AFM.

Both biomolecular pairs are experimented using conventional techniques (i.e. piezoactuation or electromagnetic actuation) with both commercial and new custom AFM system (see chapter 4.1 and chapter 4.2). Figure 4.1 shows the schematic of the single molecular force spectroscopy experiments using traditional piezo actuation method. Due to the actuation of the piezo, the bond between the biomolecules is loaded and finally breaks [2].

In this chapter, also a novel force spectroscopy technique by using the micro-particles as an actuator and the results of unbinding experiments are presented. The advantages of this novel technique over the conventional force spectroscopy methodology are demonstrated. This new technique involves magnetic particles decorated with biomolecules as actuators and a stationary cantilever functionalized with the corresponding pair as a force sensor.

4.1. Biomolecular Pulling Experiments Using Piezoactuator

Biomolecular force spectroscopy experiments were performed for both candidate pairs using conventional piezo actuation methods. Figure 4.2 shows the schematic representation of the cantilever motion along with its deflection and a sample force curve for piezo actuated force spectroscopy experiment. First, the piezo actuates the functionalized cantilever towards the sample surface covered with biomolecules until the cantilever becomes in contact with the surface (I). As it is seen the deflection signal remains constant at this phase. Then, the cantilever is pushed into the surface and deflects positively until reaching a desired contact force value in order to achieve the bond formation between the biomolecules (II). After that, the cantilever is pulled back away from the surface by the piezoactuator. If there is a bond formation between the biomolecules, cantilever bends negatively just before it comes instantaneously out off contact with the surface (III). This sudden jump on the deflection signal corresponds to the unbinding force between the biomolecular pair. After rupture occurs the cantilever returns back to its rest position (IV).

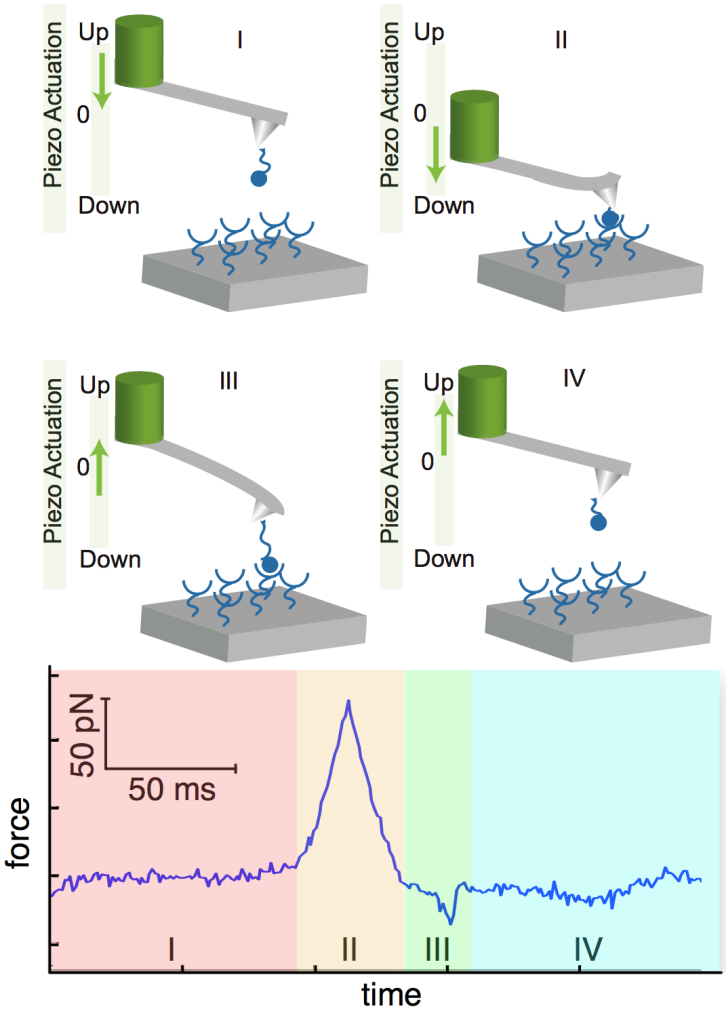

Figure 4.2. Schematic of force spectroscopy experiment using piezoactuator and obtained sample curve.

4.1.1. Biotin/Streptavidin Force Spectroscopy Using Piezoactuator

Interactions between biotin and streptavidin were probed using the new AFM system. An AFM cantilever coated with biotin (CT.BIO, Novascan, Ames, IA USA) was used during the experiments. The nominal spring constant of the cantilever is 0.01 N/m and the cantilever was calibrated for its spring constant before the experiments using thermal noise method. The calibrated spring constant was 0.0112 N/m. Biotin is covalently bonded to the tip of the commercial cantilever. Biotin coated cantilevers were then brought into contact with a substrate covered with immobilized Streptavidin (VXP0010,

Xenoprobe). Streptavidin is uniformly coated over the surface of the substrate and the molecules are covalently bonded. The measurements were performed in 100 µL-phosphate buffered saline (PBS) at room temperature. The cantilever was repeatedly actuated using the piezo in and out of contact with the substrate during the experiment. The loading rate was controlled between 10^2 and 10^6 pN/s and hundreds of approach-withdrawal cycles were obtained for each loading rate. Figure 4.3a shows a sample force curve where a specific unbinding force of 80 pN was recorded. The offset in y-axis between the approach and the retract curve is due to the hydrodynamic drag on the cantilever. Figure 4.3b shows a force curve where there is no binding/unbinding event before the cantilever was out of contact with the surface.

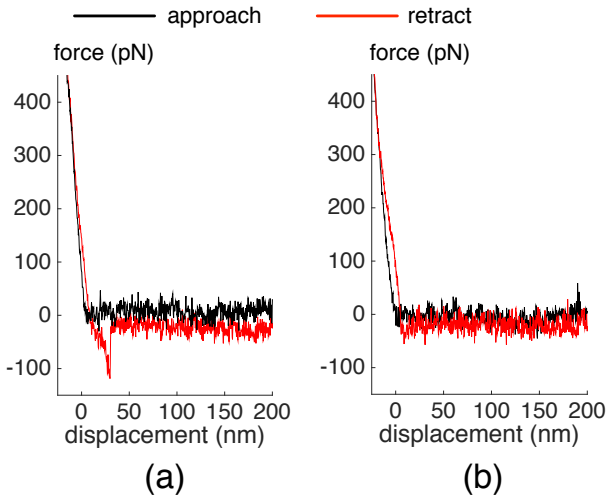

Figure 4.3. A sample force curve a) showing a biotin/streptavidin interaction unbinding force about 80 pN with a loading rate of $3.3x10^4$ pN/s b) having no unbinding event.

Figure 4.4 shows the force histograms for the data collected. Rupture forces, as a function of loading rate is presented along with the probability of specific events. The most probable rupture forces are obtained from the Gaussian fits to the force histograms at corresponding loading rates. The minimum detectable force level in this experiment was determined to be 6.8 pN in PBS by calculating the root mean square (RMS) noise in the out off contact portion of the sample force curves.

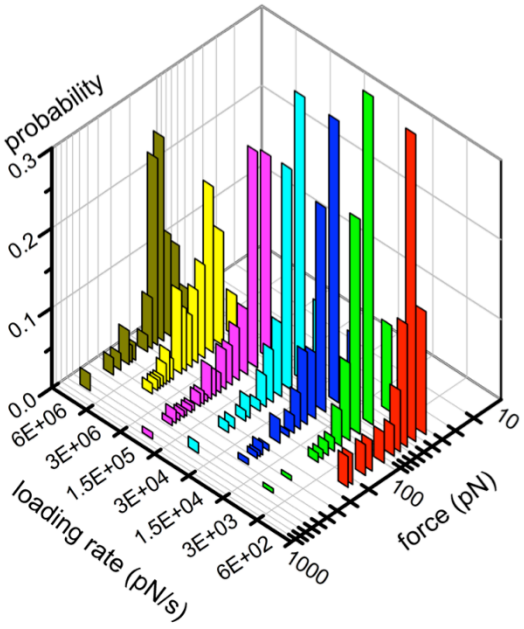

Figure 4.4. Force histograms for the unbinding force levels of single biotin/streptavidin pairs obtained using custom AFM experiment.

Biomolecular pulling experiment using biotin/streptavidin pair was also performed using a commercial AFM system (Dimension Edge, Bruker Nano, Santa Barbara, CA USA) for comparison. Same type of cantilevers (CT.BIO, Novascan, Ames, IA USA) was used for the experiment. The cantilever was actuated against a cover slip coated with streptavidin molecules. For the incubation process of the cover slip, 20 µl of streptavidin solution which has a original concentration of 10 mg/100 µl was diluted with 50 µl of buffer solution (PBS) for three times. The cover slips were incubated for 13 minutes at room temperature in the diluted streptavidin solution. Figure 4.5a shows a typical force curve indicating an unbinding event between a single pair of biotin and streptavidin molecules with a force strength of 75 pN. The probability of observing an unbinding event was approximately 40-50%. On the other hand,Figure 4.5b shows a force curve with no adhesion/rupture event. Since the biomolecular binding is a stochastic process, having a considerable percentage of force curves indicated neither adhesion nor rupture events is a justification of that the observed events are actually arising from the specific single molecular interactions.

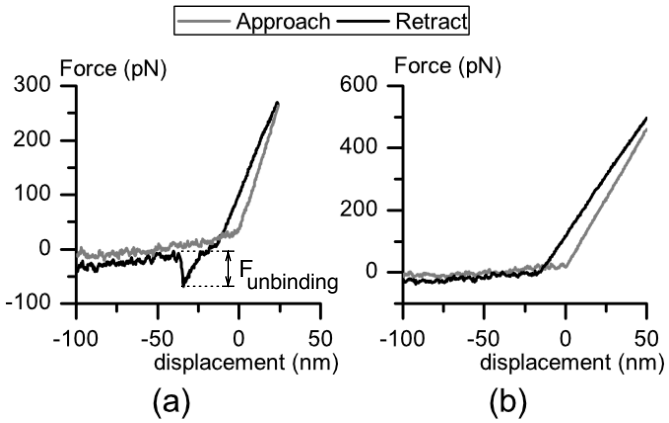

Figure 4.5. a) A typical force curve exhibiting an unbinding event with a force strength ($F_{unbinding}$) of 75 pN. b) Another force curve indicating no adhesion/rupture events.

The piezotube of the commercial AFM system was actuated at seven different speeds for the experiment. At each speed, approximately 100 force curves showing a specific interaction were recorded to obtain statistically significant data. Figure 4.6 shows the force histograms of the biotin/streptavidin bond strength at different loading rates resulting from the commercial AFM setup experiments.

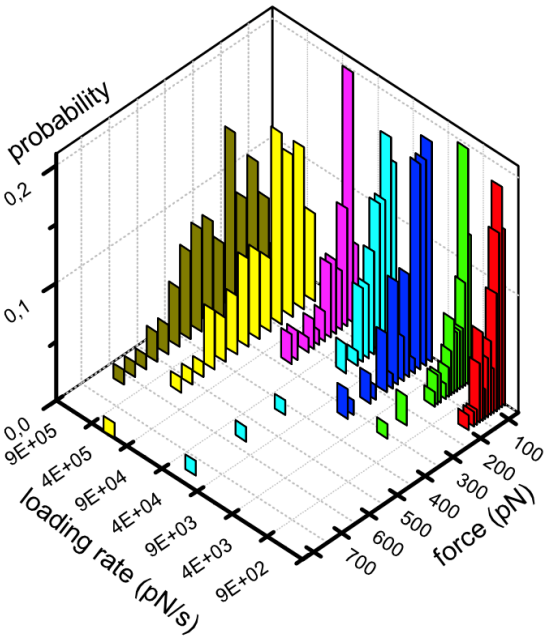

Figure 4.6. Force histograms for the unbinding force levels of single biotin/streptavidin pairs obtained using commercial AFM experiment.

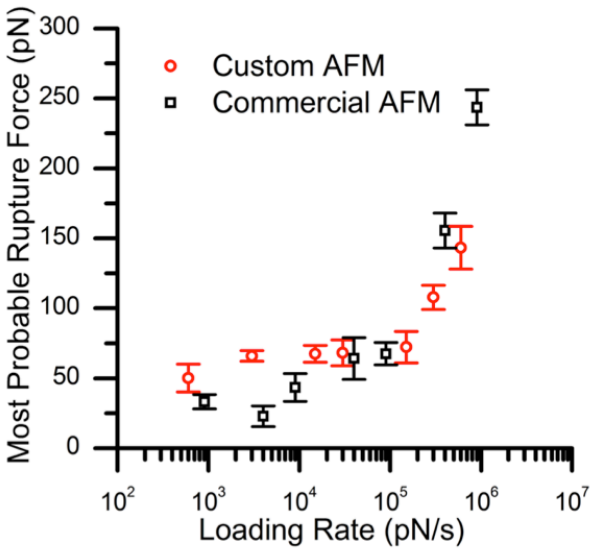

Figure 4.7. Most probable rupture force versus loading rate graph, red scatter and black scatter correspond the custom AFM measurement and Commercial AFM measurements, respectively.

Finally, the data generated using the customized AFM setup and the commercial AFM setup were combined together as shown in Figure 4.7. The most probable rupture forces corresponding to each loading rate for both experiments are calculated by fitting a Gaussian distribution curve to each data set. There is a very good agreement between the data to validate the functionality of the developed AFM setup.

Bell's parameters, i.e. the dissociation rates and width parameters of energy landscape, are extracted from the loading rate versus most probable rupture force information. The calculated parameters can be seen in Table 4.1. One can clearly see the existence of two different strength regimes of the bond rupture dependence on the logarithm of the force loading which are ranging from 10^2 to 10^6 pN/s. For small loading rates, the barrier width x_β, and off rate, k^o are calculated as 0.849 nm and $6.41\text{x}10^{-4}$ s^{-1} respectively. For higher loading rates, x_β and k^o are 0.0721 nm and $7.14\text{x}10^{2}$ s^{-1}, respectively. The results are consistent with the experimental results performed with commercial AFM (Bruker Dimension Egde results: for small loading rates: x_β and k^o are 0.484 nm and $6.04\text{x}10^{-4}$ s^{-1}, for higher loading rates: x_β and k^o are 0.0507 nm and

$5.25x10^{2}$ s^{-1}). Both sets of parameters are also in good agreement with previously published results (Yuan et. al., 2000 presented as: for small loading rates: x_β and k^o are 0.49 nm and $1.67x10^{-5}$ s^{-1}, for higher loading rates: x_β and k^o are 0.05 nm and 2.09 s^{-1}) [8, 25]. These results are very important to validate the performance of the new developed AFM setup in biomolecular force spectroscopy.

Table 4.1. Bell's parameters for biotin/streptavidin interaction.

	Small loading rates (pN/s)		High loading rates (pN/s)	
	Barrier width, x_β (nm)	Dissociation constant, k^o (1/s)	Barrier width, x_β (nm)	Dissociation constant, k^o (1/s)
Custom AFM	$8.49x10^{-1}$	$6.41x10^{-4}$	$7.20x10^{-2}$	$7.14x10^{2}$
Commercial AFM	$4.84x10^{-1}$	$6.04x10^{-4}$	$5.10x10^{-2}$	$5.25x10^{2}$

4.1.2. Heparin/FGF-2 Force Spectroscopy Using Piezoactuator

Different experimental protocols were used for these experiments. In one case, the cantilever was incubated with FGF-2, whereas the substrate was coated with heparin. The concentrations of FGF-2 and heparin were 112.5 µg/mL and 20 µg/mL, respectively. After an incubation time of 30 minutes at room temperature, the surface of the substrate was further incubated with bovine serum albumin (BSA) to avoid non-specific adhesion between the tip and the substrate. A V-shape silicon nitrate cantilever (PNP-TR, Triangular, Novascan) was used during the experiment. The nominal spring constant of the cantilever is 0.035 N/m. The cantilever was calibrated for its spring constant before biomolecular experiments. Then, force distance curves were recorded in PBS at a loading rate range from 10^3 to 10^7 pN/s.

The representative AFM force spectroscopy measurements carried out with the functionalized surfaces is shown in Figure 4.8. During the approach phase of the recording cycle (red), the AFM tip is lowered onto the cover slip with the help of piezo. No interaction is detected between the tip and the surface until they are in contact. After the cantilever and the surface are in contact, the cantilever is retracted back to its initial position (black). Figure 4.8a shows clearly when a specific event is observed. Figure 4.8b shows a force curve when the molecules are not bound to each other. The probability of adhesion was measured to be 30-40%.

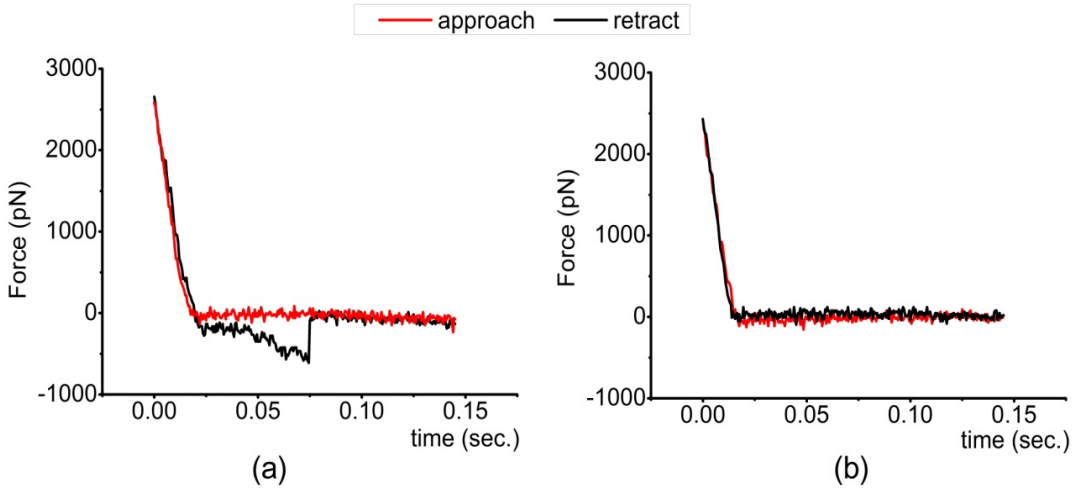

Figure 4.8. A sample force curve, a) showing a specific heparin/FGF-2 unbinding event, b) having no adhesion/rupture event.

The experiments were performed using both the customized AFM setup and the commercial AFM setup. Figure 4.9 reveals the most probable rupture forces at each loading rate. As it is seen, the commercial AFM and the custom designed AFM results are in a good agreement. This proves that the performance of the custom AFM with the conventional methods is similar to a commercial AFM. Moreover, control experiments were performed by flooding the substrate with excess FGF-2 to block heparin molecules. The probability of adhesion was reduced significantly (approximately 3%) while the force levels were similar. As a result of the control experiments, it is clear that the measured events during the experiments are specific single molecular interactions between heparin and FGF-2.

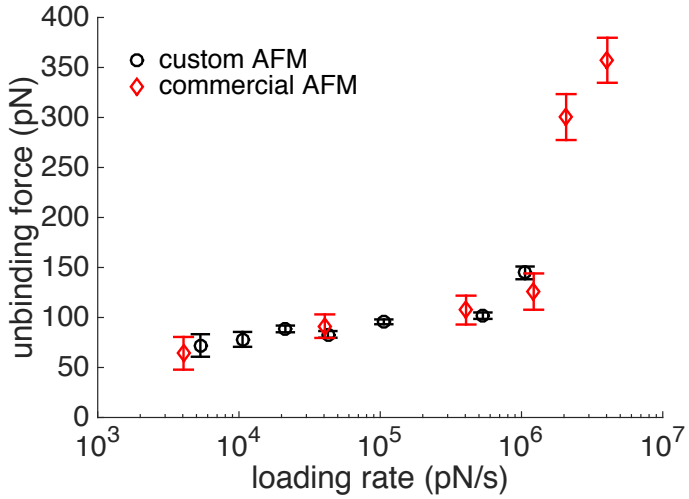

Figure 4.9. The resulting most probable rupture force versus loading rate graph of the heparin/FGF-2 unbinding experiments, performed both in custom and commercial AFM.

4.2. Biomolecular Pulling Experiments Using Magnetically Actuated Cantilevers

After completing the piezo pulling experiments, the biotin/streptavidin interaction was measured using magnetically actuated cantilever with new AFM system. To perform this experiment, a ferromagnetic bead with a diameter of 30 μm was attached to a cantilever (MLCT-C, Bruker Probes) to probe the interactions between streptavidin and biotin via magnetic actuation. The cantilever was functionalized with biotin and tested against the substrate covered with immobilized streptavidin (VXP0010, Xenoprobe) in PBS. During magnetic actuation experiments, the cantilever is brought within the vicinity of the substrate and actuated using a triangular current wave applied to the electromagnet. The schematic of the experimental methodology and sample force curves for both specific interaction and no adhesion/rupture events are shown in Figure 4.10. First, the electromagnet attracts the cantilever and the cantilever comes into contact with the substrate to allow the formation of molecular bonds. The displacement of the cantilever does not change when it is in contact with the substrate. Then the electromagnet repels the cantilever away from the substrate. Figure 4.10a shows a typical force trace where an

unbinding force of 285 pN was measured before the cantilever lost contact with the substrate. Figure 4.10b shows another force trace where no adhesion/rupture event was observed.

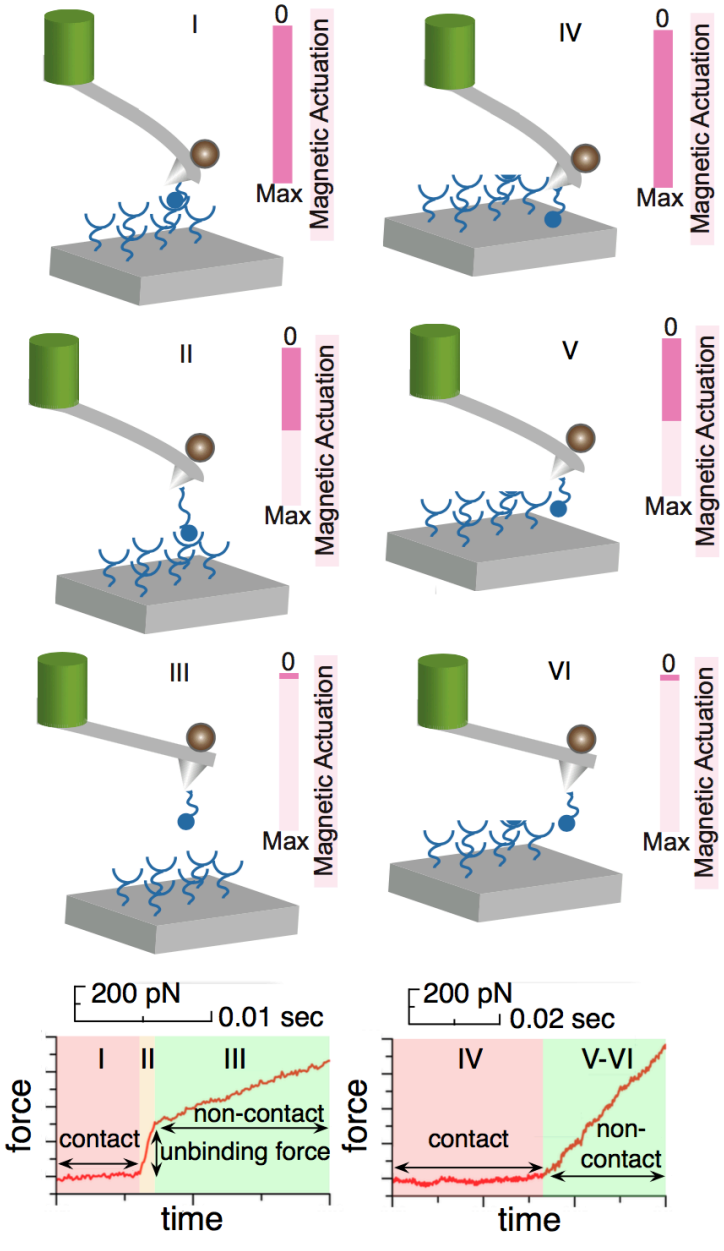

Figure 4.10. Schematic of the experimental methodology for magnetically actuated bead attached cantilever and sample force curves for both a) specific interaction between streptavidin and biotin showing 285 pN rupture force, b) no adhesion/rupture event.

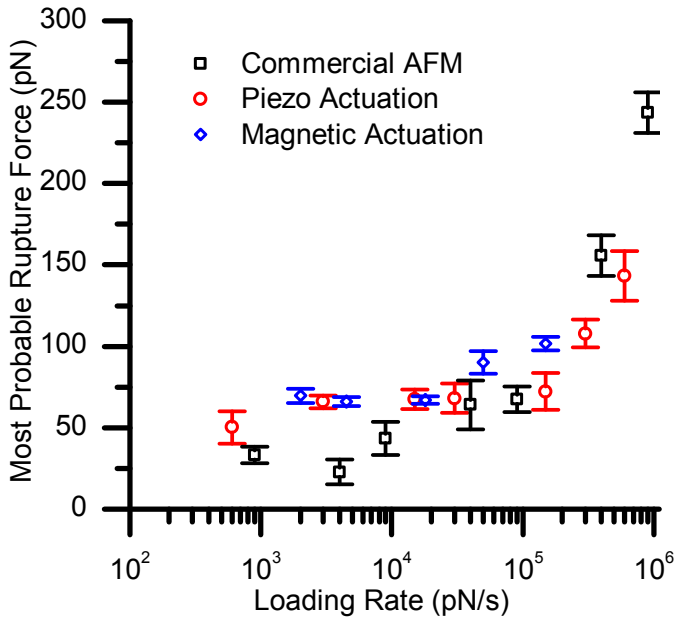

Figure 4.11. Loading rate vs. most probable rupture force obtained using piezo and magnetic cantilever actuation compared with the results of experiments obtained using a commercial AFM system.

The results of the experiments using the customized AFM setup with piezo and magnetic actuation and using the commercial AFM setup are compared, as shown in Figure 4.11. The most probable rupture forces corresponding to each loading rate for both experiments was calculated by fitting a Gaussian distribution curve to each data set. The results are in good agreement, validating the functionality of the new AFM setup using both the conventional piezoactuators and electromagnetic actuators.

4.3. Biomolecular Pulling Experiment Using Functionalized Magnetic Micropillars

The interactions between heparin and FGF-2 molecules were investigated using two different types of magnetic micropillars, having a length of 15 µm or 25 µm and a diameter of 2 µm. Both types of micropillars are composed of cobalt-nickel alloy with a gold cap to functionalize the molecules on the gold segment. Figure 4.12 schematically describes the magnetic actuation of the micropillars in sequence. First the FGF-2 functionalized

cantilever is approached to the surface, which is covered with heparin coated magnetic micropillars via piezo actuation (I-II). The micropillars have 15 µm and 25 µm length and are stand on a template with a distance. While pressing on to the surface, a micropillar may be broken (III), and Heparin on pillar may covalently bond to FGF-2 on the cantilever. After the cantilever is called back (IV), the coil is driven and pulls back the micropillar onto the surface. Electromagnetic actuation may lead to unbinding of the molecules located at the cantilever and the magnetic pillars, showing molecular rupture events, R1 and R2 (V) clearly.

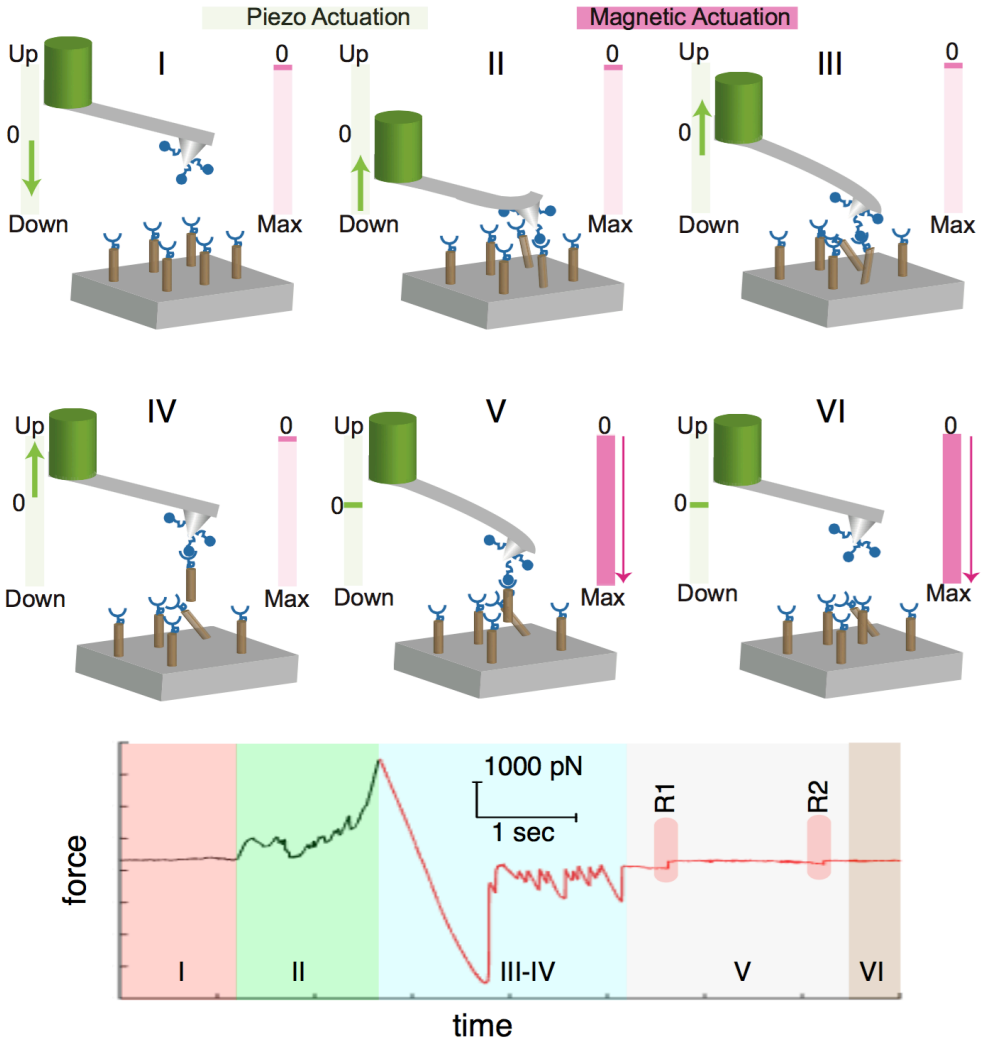

Figure 4.12. Schematic representation of the dual actuation capability of the system and a sample force curve using heparin coated magnetic micropillars against FGF-2 coated cantilever (I-VI). Multiple single molecular events (R1-R2) are resolved clearly.

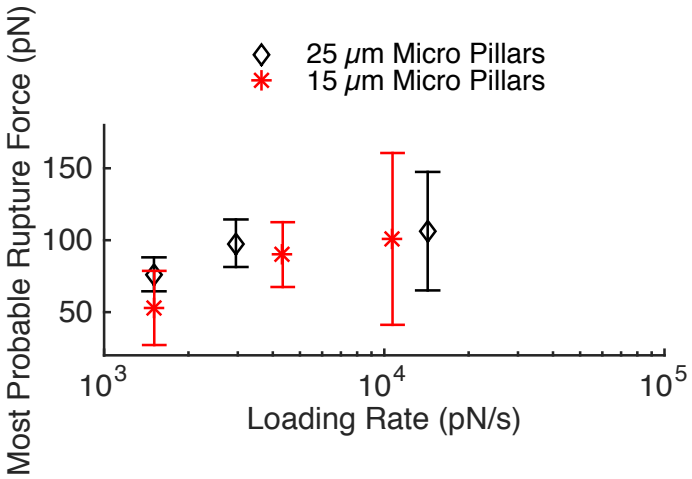

Figure 4.13. Most Probable rupture force versus loading rate graph for heparin/FGF-2 interaction performed in different days using new magnetic particle pulling technique with different size heparin labeled micropillars.

The unbinding rupture forces are obtained from 50 pN to 100 pN for the corresponding loading rates ranging from $0.5x10^4$ to $0.5x10^5$ pN/s, in Figure 4.13. The results of heparin/FGF-2 unbinding using magnetic particles are consistent for each trial using 15 μm and 25 μm of length micropillars and also in an aggrement with the piezo pulling experiments. This shows the miniaturized-magnetic particles method for force spectroscopy experiment is promising as a novel methodology.

Using the micropillar may reduce the hydrodynamic effects on the measurement via the aspect ratio of the pillar. This may provide us an advantage to reduce the loading rates lower than 10^3 pN/s and higher than 10^6 pN/s which are beyond the bandwidth of the single-molecular force spectroscopy using conventional piezoactuators. On the other hand, clustering of micropillar due to their geometric features and magnetic properties becomes a drawback for the methodology. To overcome this problem, a similar methodology is developed using magnetic micro-beads. Due to their super-paramagnetic properties and symmetrical geometries the clustering problem is minimized during the single-molecule pulling experiments. (see chapter 4.4).

4.4. Biomolecular Pulling Experiment Using Functionalized Magnetic Micro-Beads

The interactions between the both biomolecular pairs were also measured using functionalized magnetic beads and functionalized cantilevers via a new methodology with dual actuation of electromagnet and piezo. This new experimental methodology is schematically shown in Figure 4.14.

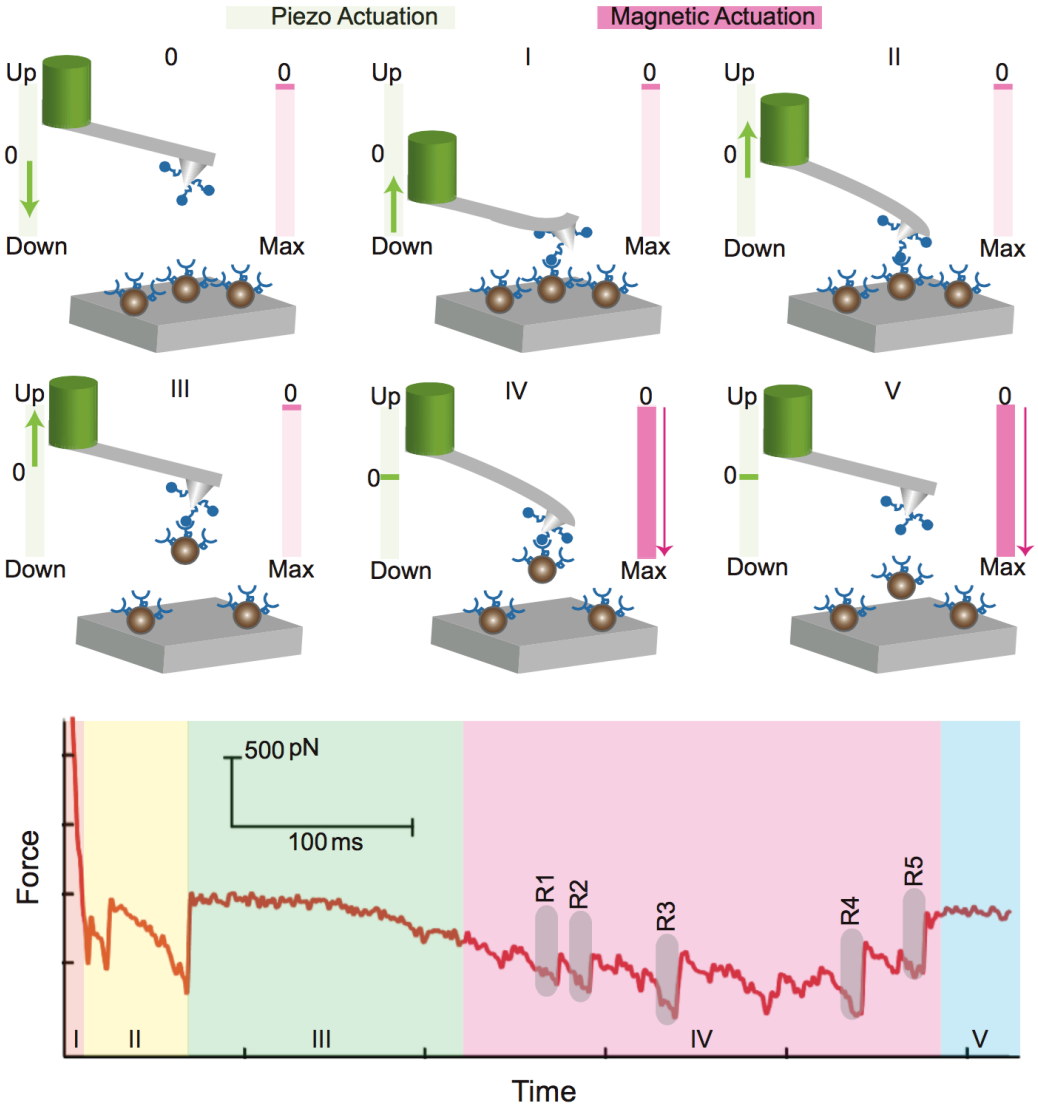

Figure 4.14. Schematic representation of the dual actuation capability of the system (0-V) and a sample force curve obtained during a biomolecular experiment. Multiple single molecular events (R1-R5) during phase 4 are resolved clearly.

First, the functionalized cantilever is brought down using the piezo actuator to the substrate, which is covered with labeled magnetic beads (0). The cantilever is first pressed into the substrate to allow molecules to form bonds. Then, the cantilever is pulled away from the substrate using the piezoactuator (I). As the cantilever goes out of contact with the substrate, non-specific adhesions can be observed (II). Finally, the cantilever goes completely out of contact and then the piezo actuator stops (III). After the piezo actuator is turned off, the electromagnet is driven to pull the magnetic beads back to the substrate (IV). Electromagnetic actuation may lead to unbinding of the molecules located at the cantilever and the magnetic beads, showing molecular rupture events. (IV). Multiple single molecular rupture events labeled as R1-R5 are observed in region IV while the coil is on. The unbinding forces of the rupture events are ranging from 100 pN to 500 pN on the specific force curve. One of the main advantages of this novel method is the capability to resolve multiple events using magnetic bead actuation. This is due the following fact that the surface of the cantilever tip can accommodate multiple beads. The last phase (V) on the force curve indicates all the beads are detached from the cantilever.

4.4.1. Biotin/Streptavidin Force Spectroscopy Using Streptavidin Labeled Magnetic Beads

The interactions between the biotin and streptavidin pairs were also measured using functionalized magnetic beads (Streptavidin coated, 2.8 μm of diameter, Dyna Beads) and the biotin-coated cantilever (CT.BIO, Novascan, Ames, IA USA) using a new methodology with dual actuation of electromagnet and piezo. This new experimental methodology is schematically shown in Figure 4.14. The surface was covered with 5 μl diluted Dyna Beads solution and the experiment was performed inside 100 μl PBS solution.

Figure 4.15a shows the force histogram results of streptavidin labeled magnetic bead pulling experiments. The histograms contain more than a hundred curves for each specific loading rate. As seen in Figure 4.15b, the most probable rupture forces versus loading rate graph was obtained from the Gaussian fits to the force histograms at corresponding loading rates. After presenting the result of the specific interactions between biotin and

streptavidin, the same experiment was performed as a control experiment by saturating biotin on cantilever with excess streptavidin. As a result of the control experiment, the probability of specific interaction fall down to a value of less than 1%. With the performed control experiment, it was validated that measured unbinding forces are specific interactions. In addition, the new method is validated with the results obtained using the conventional methods. (see chapter 4.1.1)

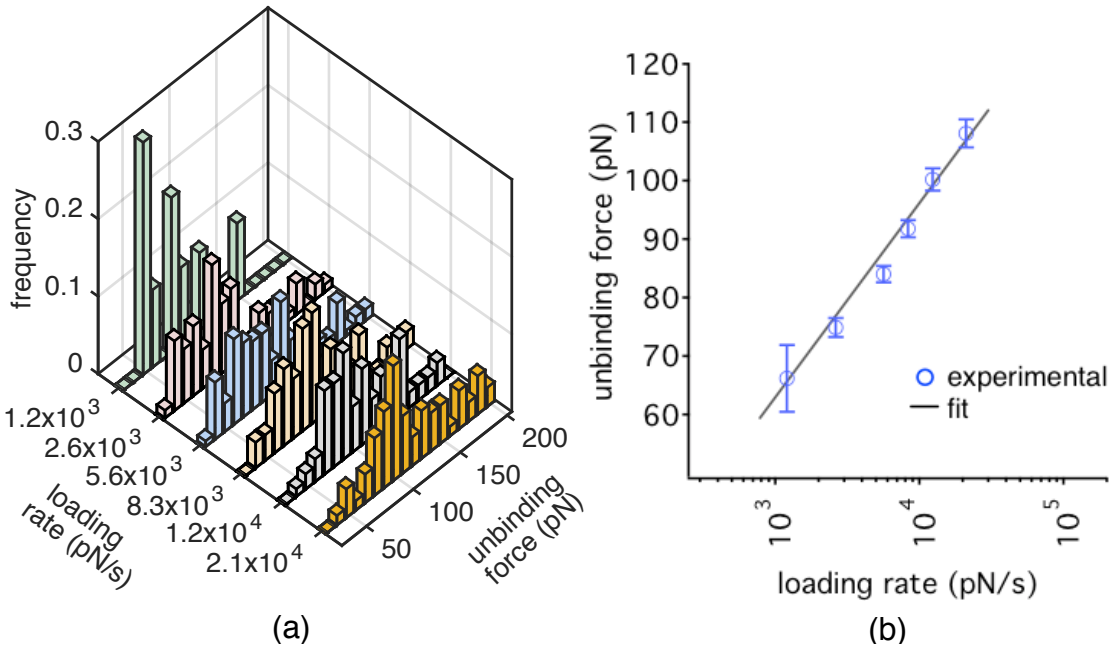

Figure 4.15. a) Force histograms for biotin/streptavidin from magnetic bead pulling experiments b) Most probable rupture force versus loading rates for biotin/streptavidin interaction.

4.4.2. Heparin/FGF-2 Force Spectroscopy Using Heparin Labeled Magnetic Beads

In addition to magnetic micropillar pulling experiments, interaction between the heparin/FGF-2 pair was measured using dual actuation technique with labeled magnetic beads. The experimental methodology is similar with one explained in Figure 4.14. An AFM cantilever made of silicon nitride with nominal spring constant of 0.01 N/m (MLCT-C type, V shaped Silicon Nitride cantilever, Bruker) was used for the experiment.

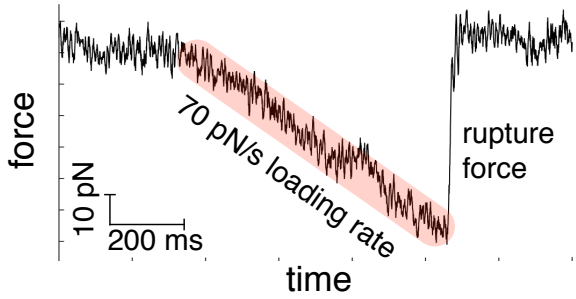

Figure 4.16. A sample force curve with 70 pN/s loading rate and showing 50 pN rupture force, from the biomolecular interaction between the heparin labeled magnetic bead and FGF-2 labeled cantilever.

Cantilever was incubated in FGF-2 (Fibroblast Growth Factor 2) with a concentration of 112.5 μg/ml for 30 minutes at room temperature, and tested against heparin coated magnetic beads with a diameter of 3.0 μm (with the surface coating of PEG-NH2, micromer®-M, Micromod). The commercial beads were functionalized with heparin. Then the heparin-coated beads were injected into a 100-μL droplet of PBS (Phosphate Buffered Saline) on the sample surface of the AFM, which was covered with 50- μl of BSA solution (Bovin Serum Albumin) for 30 minutes and then washed removing excess BSA to avoid non-specific adhesions. Several hundreds of force curves were collected at different loading rates using the magnetic actuator. A typical force-distance curve resulting in a rupture force of 50 pN at a loading rate of 70 pN/s is depicted in Figure 4.16.

With the new miniaturized-magnetic particle actuation method it becomes possible to reach the loading rate around 10^1 pN/s, since the negative effects of drift due to large the mechanical loop and large actuators are minimized. Data points labeled with black circles of Figure 4.17 shows the most probable rupture forces collected for various loading rates (50 pN/s - 7000 pN/s) using magnetic actuation method.

Another single molecule experiment was also performed using the piezo actuator of our custom AFM setup to actuate the cantilever. Cantilevers (Nanoworld PNP-TR, with

nominal stiffness 0.08 N/m) were incubated in an identical FGF-2 solution for 30 minutes at room temperature. These cantilevers were tested against cover slip, which was incubated with heparin with a concentration of 20-µg/ml at room temperature. Then, the excess heparin was washed from the cover slips and the coverslip was incubated for 30 minutes with 50-µl of BSA, which was washed away after incubation to avoid non-specific interactions. Finally, the experiment was performed in 100-µL droplet of PBS. During the experiments, the piezo was actuated using a triangular wave at various speeds to induce different loading rates. Data points labeled with red stars of Figure 4.17 represents the most probable rupture forces between heparin and FGF-2 at different loading rates obtained using the piezo actuator of our custom AFM.

Finally, another single molecular pulling experiment between these two molecules was performed using a commercial AFM system (Dimension Edge, Bruker). Again a cantilever (Nanoworld PNP-TR, with nominal stiffness 0.08 N/m) was incubated using the identical FGF-2 solution and actuated over a cover slip, which was incubated with heparin and BSA using the same methodology with the previous experiments. The resulted most probable rupture forces between heparin and FGF-2 at different loading rates are presented with blue triangles in Figure 4.17.

All the results of these three experiments are in a good agreement with each other as shown in the fitted lines to the data points. Comparing the novel method with conventional methods proves the functionality of the custom system and new technique for the single molecular force spectroscopy experiments. According to combined results, the method of magnetic bead actuation is advantageous at lower loading rates as the drift in the system can be minimized by shrinking the size of the actuators and breaking the mechanical loop between the cantilever and a rigid substrate surface (see chapter 3.3.2). At least two order smaller loading rates were achieved using miniaturized-magnetic particle actuation method compared to the results with traditional piezo actuation using both custom and commercial AFM. That is very important to understand the dynamical behavior of the molecules around physiological loading rates, which are lower than the loading rates measured with the conventional AFM techniques.

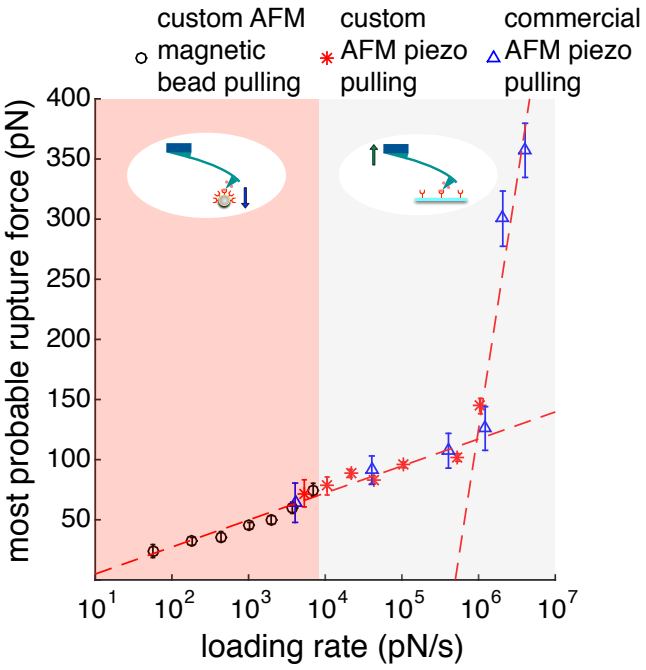

Figure 4.17. Rupture force vs. loading rates graph for heparin and FGF-2 pulling experiments using magnetic bead actuation (black circles), piezo actuation (red stars) on the custom AFM setup and on a commercial AFM system (Dimension Edge, Bruker).

4.4.3. Heparin Labeled Magnetic Beads Control Experiments

The probability of the specific ruptures between heparin and FGF-2 was found 29.1% for the repeated experiments, using magnetic bead actuation technique (Figure 4.18). The following control experiments were also carried out to specify the activity of heparin molecule. For the first control experiment, the same experimental procedure was followed except the increase of the salt concentration of the buffer solution with addition of NaCl. Under these circumstances, it is expected FGF-2 molecules, which is not binding anymore to Heparin ones. It is seen the probability of the ruptures lowered to 6.8% with the addition of the NaCl into the buffer solution. For the second control experiment, the functionalized cantilever was kept inside the heparin solution for a long time in order to saturate the FGF-2 molecules with heparin ones. As it is expected, the probability of the binding activity has reduced to the 1.9% for the corresponding control experiment. For the last control measurement, the blank beads were used instead of heparin coated ones. As we

have discussed before, heparin molecules are embedded onto the magnetic beads in realistic measurement protocol. The following control experiment was performed with blank beads in order to discriminate the non-specific adhesion, which is found about 1.6% after calculations. As a result of all of these control experiments, it is demonstrated that this novel magnetic particle actuation technique is adequate to measure single molecular interactions between the biomolecular pairs, like heparin/FGF-2.

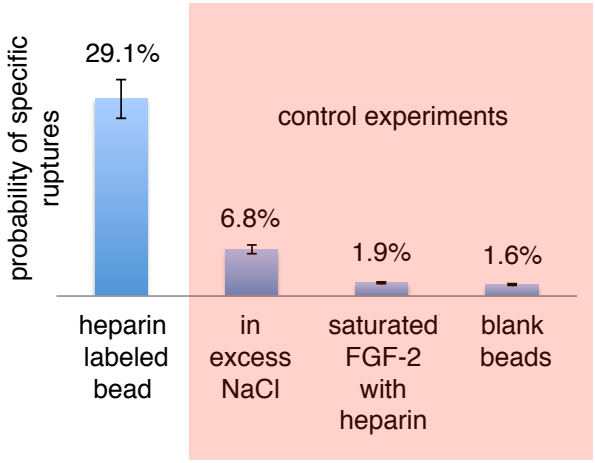

Figure 4.18. Probability of Rupture force for heparin and FGF-2 single molecular interaction and control experiments using magnetic bead pulling technique.

4.4.4. Effect of pH on Heparin/FGF-2 Unbinding Forces

In order to investigate the electrostatic interaction of heparin/FGF-2, the measurements were repeated at three different pH values of PBS solution. A significant number of force-curves were collected at enough range of loading rates (50 pN/s-7000 pN/s). The most probable rupture forces are depicted in Figure 4.19 at pH 5.5, pH 7.5, and pH 8.5, respectively. An increase in the rupture force is seen in the measurement, which is performed at pH 5.5. The trend of the rupture forces on the measurement done at pH 8.5 is slightly smaller than ones measured in pH 7.5. It is a very important result since the pH value of cells with cancer is smaller than the pH value of healthy cells.

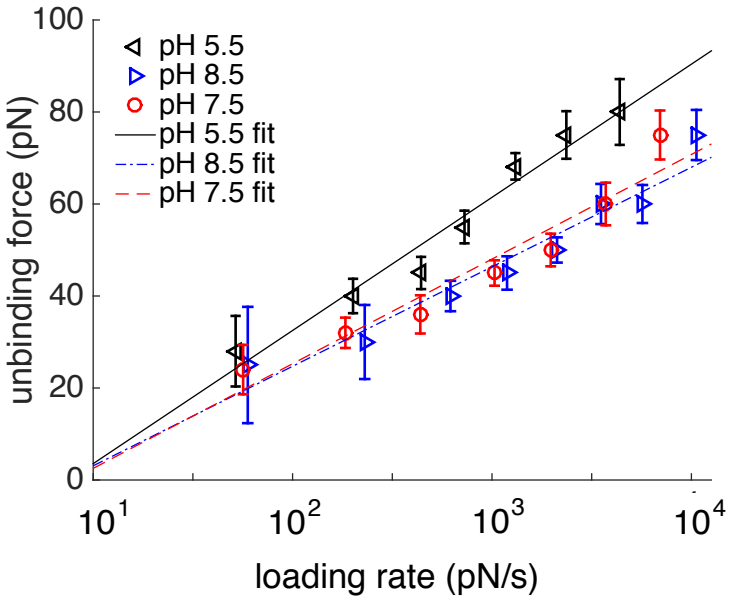

Figure 4.19. The most probable rupture force vs. loading rates graph for heparin and FGF-2 single molecular interaction. Each labels represents the experiments, which are carried out in different pH values of PBS solution using magnetic bead pulling technique.

4.4.5. Biomolecular Force Clamp Experiment without any Feedback Mechanism

Force clamp measurements are another type of single molecular experiment to understand the dynamics of molecular interactions between the biomolecules. In conventional force clamp methods, after forming the bond between the biomolecule on the cantilever and the counter interacting biomolecule on the substrate by pressing cantilever over the surface, the cantilever is pulled back using the piezoactuator to apply a specific constant force, i.e. clamping force, on the biomolecular bond between the pair. However, the drift on the cantilever results fluctuations on clamping force due mechanical loop. Therefore, a feedback loop is needed to keep the deflection signal, hence clamping force, constant. To accomplish that, the piezoactuator changes the displacement of the cantilever according to the feedback from the deflection signal until the rupture between biomolecules occurs.

This method is used for measuring the clamping time from the application of force until the rupture of the biomolecular interaction, i.e. lifetime, under the effect of a constant clamping force. With the application of this methodology, the most probable lifetime for a specific clamping force is measured. Since the lifetime is decreasing with increasing clamping force it is important to use different amount of clamping force in order to investigate the relation.

As an inherent advantage, performing force clamp experiments without any need for feedback is possible using the magnetic bead actuation method. The force applied on magnetic beads is constant when the electromagnet is driven with a constant current signal. The current applied to the electromagnet determines the strength of the magnetic field that determined the force applied to the beads. Right after the functionalized cantilever grabs a magnetic bead, a constant force is applied on the bead until a rupture event is observed. The duration of time between the instance when the force is applied and the instance of rupture, i.e. lifetime, is recorded. Force-clamp experiments were performed between heparin on magnetic beads and FGF-2 on the cantilever using this method.

A typical heparin-FGF-2 force clamped data in is shown in Figure 4.20. We set a clamping force of 60 pN and measured a life-time of 600 ms. The reason behind that having a force level different that the zero after rupture occurs is the existence of a second bead on the cantilever tip. The RMS noise for the clamping portion of this specific experiment is 3.13 pN, showing that the force clamp experiment with the magnetic particle actuators has a considerably stable clamping force.

Force clamp experiments are also important to understand the single molecular dynamics. In a conventional AFM methodology force clamp experiment are performed using piezoactuator with an active feedback to compensate the drift in the cantilever during the clamping time, since drift on the cantilever results the fluctuations on clamping force due to the mechanical loop. However, magnetic particle actuation methods eliminates the drift problem by breaking the mechanical loop and achieves constant clamping force by applying constant current to the electromagnet. Therefore, this technique offers improved force clamp measurements.

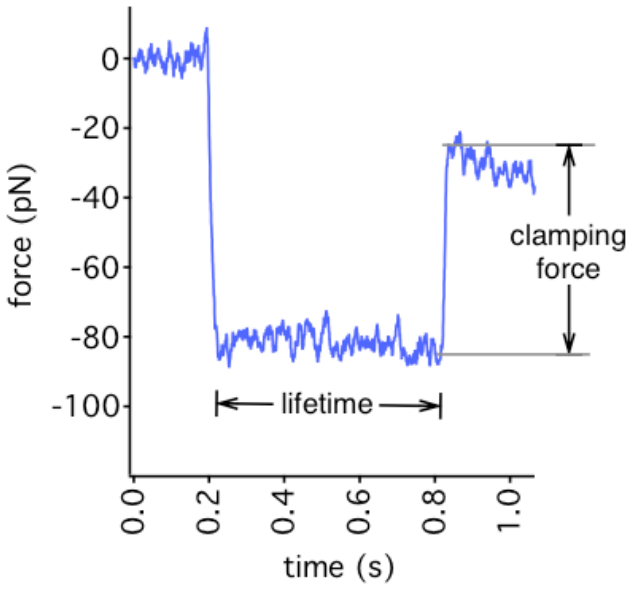

Figure 4.20. A sample force clamp curve for heparin vs. FGF-2 interaction, obtained by applying a step magnetic force to the heparin labeled magnetic beads, without any feedback loop requirements.

5. CONCLUSION

In this thesis, design and characterization of a new AFM setup having conventional piezoactuator together with an electromagnetic actuator and a novel AFM technique with dual actuation capability for biomolecular force spectroscopy and force clamp experiments are presented.

The custom AFM system composed of basically two parts as AFM head and coil/sample holder is manufactured from a rigid polymer using stereolithography technique (Rigid Opaque from Stratasys Ltd., MN, USA) to make required mechanical modifications easy. A PXI embedded controller (NI PXI-8102, National Instruments, TX, USA) having 8 analog input and 2 analog output channels and 1.25 MS/s sampling rate is programmed in NI-LabVIEW environment and used to drive the system in characterization and biomolecular experiments.

Characterization experiments are performed for AFM head and the electromagnetic actuator system both separate and together to demonstrate the performance levels. Using a commercial AFM cantilever (SNL10-D triangular, Bruker probes), integrated noise levels for AFM head are measured as 2 pN in air, and 3 pN in water within 1 kHz detection bandwidth, which is adequate to measure the unbinding events between biomolecules. Performed Eigenfrequency analysis (using Comsol Multiphysic 4.3b) to distinguish the mode shapes of the AFM head predicts the Eigenfrequency of the adaptor part with 10.5 % error compared to the experimental results.

In addition on the electromagnetic actuator side, a flux density of over 0.55 Tesla is achieved at a working distance of 100 μm from the pole-piece with a FeCo core. This amount of flux density is adequate to actuate the magnetic particles during the biomolecular experiments. Driving the electromagnet at 1 kHz with a square signal having 300 mA amplitude, results 7.5 nN force on the commercial MFM cantilevers (MESP, rectangular, Bruker probes). The electromagnetic force response for the same cantilever has a cutoff frequency around 1 kHz whereas the cutoff frequency for current response of

the coil is around 3 kHz. The force response decays faster than the current response because of the lowering of effective permeability due to hysteretic and eddy current losses in the core material. The bandwidth of the force response can be significantly increased using the ferrite core, which has lower hysteretic and eddy current losses, albeit at the cost of overall reduced force, because of its lower saturation induction (Ms ~ 0.4T)

The temperature stabilization is extremely important for biomolecular experiments since temperature induced deflections on cantilever result in drift during the experiments. After manufacturing the coil/sample holder from aluminum, experimental measurements shows the temperature inside the experimental meniscus can be stabilized within 0.1° C with the use of the water-cooling system and a Peltier cooler (TEC).

Single-molecule experiments have been performed using the new AFM system. Different pairs of biomolecules are selected as a candidate to conduct experiments using different force spectroscopy techniques. As the first candidate, the biomolecular interaction between biotin and streptavidin, which is a well-known pair in the literature, is investigated. As second candidate, heparin/fibroblast growth factor-2 (FGF-2) interaction is investigated. Both biomolecular pairs are experimented in a range of loading rate between 10^3 pN/s and 10^6 pN/s using conventional force spectroscopy techniques (i.e. piezoactuation or electromagnetic actuation) with both commercial and custom AFM system. The results are in good agreement with each other and the literature.

After proving the results using commercial AFM and conventional methods, a novel AFM technique with dual actuation capability is presented in this thesis. In this new approach, magnetic particles (i.e. microbeads, micropillars) are used as a secondary actuator together with the conventional piezoactuator. Using magnetic beads minimizes the size of the actuator down to a size comparable to that of a single molecule. Using miniaturized actuators improves the system dynamics by reducing the hydrodynamic drag forces drastically. Reduced hydrodynamic drag improves force resolution and the stability of the system significantly.

In addition, bead actuation technique substantially decreases the drift in the AFM measurements and also provides biomolecules from crushing, since the large mechanical

loop between the cantilever and the substrate is broken. As a result of these improvements, a loading rate as order 10^1 pN/s is achieved in single molecular force spectroscopy with the new AFM system and the novel methodology. Use of this novel biomolecular measurement technique increased the bandwidth of force spectroscopy application at least two order of magnitude according the loading rate as compared the conventional AFM methods. Moreover, resolution of multiple-single molecular event is increased since each magnetic particle inside the meniscus can be act as a free actuator.

In this thesis also the pH dependence on unbinding forces is demonstrated for heparin/FGF-2 pair. As a result of this experiment, it is seen that a decrease in the value of pH results an increase in the unbinding forces. It is a very important result since the pH value of cells with cancer is smaller than the pH value of healthy cells.

In addition to that, magnetic particle actuation technique provides an inherited advantage on force clamp measurements. Since applying constant current to the electromagnets results constant clamp force, force clamp experiments can perform with out any need for feedback. In the force clamp experiment between the heparin and FGF-2, the RMS noise level is calculated as 3.13 pN considering the clamping portion for 60 pN clamping force.

As recommendation:

- Considering design of AFM head, integration with an optical microscope is important to see inside the experimental meniscus during the sample preparation and experiments. Although the performance level of AFM head manufactured using stereolithography is adequate to conduct the single molecular experiments, an optimized AFM head can be machined from a non-magnetic material.

- Electromagnetic actuator can be modified using litz wire to improve the frequency response of the coil. With this improvement, it is possible to reach much higher loading rates in single-molecule force spectroscopy experiments. Moreover the sample holder can be separated from the coil holder and integrated with the AFM head. As a result of this, the coil becomes independent from the sample and changing

the alignment of coil changes direction of applied force. In addition, integrating the system with a multiple degree electromagnetic manipulator is convenient to apply torque on biomolecules by twisting the magnetic particles under magnetic field.

- The software design can be modified for high-speed applications using realtime controller.

- In the experimental methodology side, magnetic particle actuation technique can be performed with different types of magnetic particles according to the needs of experiments. For illustration, particles with high aspect ratio can be used to high-speed applications since increasing aspect ratio decreases the hydrodynamic drag on the particle. Moreover, a template including grids for micro-particles can be designed for the experiments to specify the exact location of the particles and avoid clustering of them.

REFERENCES

1. *A practical guide to AFM force spectroscopy and data analysis*, Technical Note, JPK Instruments AG, 1-8, 2014.

2. Neuman, K.C., Nagy, A. "Single-molecule force spectroscopy: optical tweezers, magnetic tweezers and atomic force microscopy", *Nature methods*, Vol. 5, p.491, 2008.

3. Puchner, E.M., Gaub, H.E., "Force and function: probing proteins with AFM-based force spectroscopy", *Current opinion in structural biology*, Vol. 19, pp. 605-614, 2009.

4. Müller, D.J., Dufrene, Y.F., "Atomic force microscopy as a multifunctional molecular toolbox in nanobiotechnology", *Nature nanotechnology,* Vol. 3 ,pp. 261-269, 2008.

5. Popa, I., Kosuri, P., Alegre-Cebollada, J., Garcia-Manyes, S., Fernandez, J.M., "Force dependency of biochemical reactions measured by single-molecule force-clamp spectroscopy", *Nature protocols*, Vol. 8, pp.1261-1276, 2013.

6. Scholl, Z.N., Li, Q., Marszalek, P.E., "Single molecule mechanical manipulation for studying biological properties of proteins, DNA, and sugars", *Wiley Interdisciplinary Reviews: Nanomedicine and Nanobiotechnology*, Vol. 6, pp.211-229, 2014.

7. Torun, H., Finkler, O., Degertekin, F., "Athermalization in atomic force microscope based force spectroscopy using matched microstructure coupling", *Review of Scientific Instruments,* Vol. 80, p.076103, 2009.

8. Sevim, S., Tolunay, S., Torun, H., "Micromachined sample stages to reduce thermal drift in atomic force microscopy", *Microsystem Technologies*, Vol. 21, pp.1559-1566, 2015.

9. Beyder, A., Spagnoli, C., Sachs, F., "Reducing probe dependent drift in atomic force microscope with symmetrically supported torsion levers", *Review of Scientific Instruments,* Vol. 77, pp.056103–056105, 2006.

10. Weafer, P.P., McGarry, J.P., van Es, M.H., Kilpatrick, J., Ronan, W., Nolan, D.R., Jarvis, S.P., "Stability enhancement of an atomic force microscope for long-term force measurement including cantilever modification for whole cell deformation", *Review of Scientific Instruments*, Vol. 83 pp. 093709–093710, 2006.

11. Wenzler, L., Moyes, G., Beebe, T., "Improvements to atomic force microscopy cantilevers for increased stability", *Review of Scientific Instruments,* Vol. 67, pp. 4191–4197, 1996.

12. Altmann, S.M., Lenne, P.F., Heinrich Horber, J.K., "Multiple sensor stabilization system for local probe microscopes", *Review of Scientific Instruments.* Vol. 72, pp. 142–149, 1996.

13. Choy, J.L., Parekh, S.H., Chaudhuri, O., Liu, A.P., Bustamente, C., Footer, M.J., Theriot, J.A., Fletcher, D.A., "Differential force microscope for long time-scale biophysical measurements", *Review of Scientific Instruments,* Vol. 78, pp. 043711–043716, 2007.

14. Carrasco, C., Ares, P., de Pablo, P.J., Gómez-Herrero, J., "Cutting down the forest of peaks in acoustic dynamic atomic force microscopy in liquid", *Review of Scientific Instruments,* Vol. 79, p.126106, 2008.

15. Janovjak, H., Struckmeier, J., Müller, D., "Hydrodynamic effects in fast AFM single-molecule force measurements", *European Biophysics Journal,* Vol. 34, p. 91-96, 2005.

16. Sarangapani, K., Torun, H., Finkler, O., Zhu, C., Degertekin, L., "Membrane-based actuation for high-speed single molecule force spectroscopy studies using AFM", *European Biophysics Journal*, Vol. 39, pp. 1219-1227, 2010.

17. Vančura, C., Lichtenberg, J., Hierlemann, A., Josse, F., "Characterization of magnetically actuated resonant cantilevers in viscous fluids", *Applied Physics Letters*, Vol. 87, p.162510, 2005.

18. Stahl, S.W., Puchner, E.M., Gaub, H.E., "Photothermal cantilever actuation for fast single-molecule force spectroscopy", *Review of Scientific Instruments,* Vol. 80, p. 073702, 2009.

19. Degertekin, F.L., Hadimioglu, B., Sulchek, T., Quate, C.F., "Actuation and characterization of atomic force microscope cantilevers in fluids by acoustic radiation pressure", *Applied Physics Letters*, Vol. 78, pp. 1628-1630,2001.

20. Zhang, J., Czajkowsky, D.M., Shen, Y., Sun, J., Fan, C., Hu, J., Shao, Z., "Bias controlled capacitive driven cantilever oscillation for high resolution dynamic force microscopy", *Applied Physics Letters,* Vol. 102, pp. 073110, 2013.

21. Rankl, C., Pastushenko, V., Kienberger, F., Stroh, C.M., Hinterdorfer, P., "Hydrodynamic damping of a magnetically oscillated cantilever close to a surface", *Ultramicroscopy*, Vol. 100, pp. 301-308, 2004.

22. Jayanth, G.R., Jeong, Y., Menq, C.H., "Direct tip-position control using magnetic actuation for achieving fast scanning in tapping mode atomic force microscopy", *Review of Scientific Instruments*, Vol. 77, p. 053704, 2006.

23. Kühner, F., Lugmaier, L.A., Mihatsch, S., Gaub, H.E., "Print your atomic force microscope", *Rev Sci Instrum*, Vol. 78, p. 075105, 2007.

24. Merkel, R., Nassoy, P., Leung, A., Ritchie, K., Evans, E., "Energy landscapes of receptor–ligand bonds explored with dynamic force spectroscopy." *Nature* Vol. 397, no. 6714, pp. 50-53, 1999.

25. Yuan, C., Chen, A., Kolb, P., Moy, V.T., "Energy landscape of streptavidin-biotin complexes measured by atomic force microscopy", *Biochemistry,* Vol. 39, pp.10219–10223, 2000.

26. Klagsbrun , M., "The fibroblast growth factor family: Structural and biological properties", *Prog. Growth Factor Res*. Vol. 7, pp. 207-235, 1989.

27. Yayon, A., Klagsbrun , M., Esko, J., D.,Leder, P., and Ornitz, David M., "Cell Surface, Heparin-like Molecules are Reguired for Binding of Basic Fibroblast Growth Factor to Its High Affinity Receptor". *Cell*, Vol. 64, pp. 841-848, 1991.

28. Pokki, J., Ergeneman, O., Sevim, S., Enzmann, V., Torun, H., Nelson, B.J., "Measuring localized viscoelasticity of the vitreous body using intraocular microprobes", *Biomedical Microdevices*, Vol. 17, pp.1-9, 2015.

29. Gabrielson, T.B., "Mechanical–thermal noise in acoustic and vibration sensors" *IEEE Trans Electron Devices*, Vol. 40, pp.903-9, 1993.

30. van den Hoop, M. A. G. T., Benegas, J. C., "Colloids and Surfaces A: Physicochemical and Engineering Aspects", *Colloids and Surfaces A: Physicochemical and Engineering Aspects*, Vol. 170, pp. 151-160, 2000.

31. Dey, A., Szoszkiewicz, R., "Complete noise analysis of a simple force spectroscopy AFM setup and its applications to study nanomechanics of mammalian Notch 1 protein", *Nanotechnology*, Vol. 23, No.17, p. 175101, 2012.

32. Isikman, S.O., Urey, H., "Dynamic modeling of soft magnetic film actuated scanners. Magnetics", *IEEE Transactions*, Vol. 45(7), pp.2912-2919, 2009.

33. Cropico, "A guide to temperature measurements" http://www.seaward.co.uk/downloads/Guide%20to%20temperature%20measurement.pdf, accessed at May 2016.

34. Bell, G.I., "Models for the specific adhesion of cells to cells", *Science*, Vol. 200, No. 4342, pp.618-627, 1978.

35. Evans, E., Ritchie, K., "Dynamic strength of molecular adhesion bonds". *Biophysical journal*, Vol.72, No.4, p.1541, 1997.